SCUOLA
NORMALE
SUPERIORE

Faculty of Sciences
PhD in Chemistry

Modeling transport properties of molecular devices by a novel computational approach

Candidate
Michele Visciarelli

Supervisors
Prof. Vincenzo Barone
Prof. Ivo Cacelli
Dott. Alessandro Ferretti

October 2013

Contents

Chapter 1

Introduction

It might be just a drop in the ocean,
but tomorrow it could flavour
someone's salad.

Caterina Buscaglione

Gordon Moore, in 1965, predicted that the number of transistors per square centimetre of Silicon should have doubled every 18 months. Such prediction has been proved accurate until now, and it has become a sort of a "law" in integrated circuit miniaturization (the famous Moore's Law[1]), with academical and industrial efforts directed in making the "law" valid as long as possible. This requires that the size of transistors and the interconnecting wires between them decrease at the same rate, which, until now, has been possible with the introduction of more and more precise photolitographic techniques (capable of defining smaller and smaller patterns in which fabricate Silicon transistors, with dimensions in the order of tens of nanometers each), and the use of innovative materials both for the devices themselves and for the interconnections (such as high-K dielectrics for the transistors or Copper for the interconnec-

tions). However, in the near future, the fundamental limits rooted in the technology currently used to build transistors (Complementary Metal-Oxide-Semiconductor technology, or CMOS technology) will be reached, and new technological solution should be sought in order to try to maintain the validity of the Moore's Law as long as possible. For 50 years, the idea of using fundamental nanoscale component to build computers has been investigated. The first hint in the future direction of nanoscale science for electronics was given by Richard Feynman in his 1959 lecture entitled "There's plenty of room at the bottom",[2] which is considered by some people as one of the "starting point" in the field of nanotechnology:

> *I dont know how to do this on a small scale in a practical way, but I do know that computing machines are very large, they fill rooms. Why can't we make them very small, make them of little wires, little elements and by little I mean little. For instance, the wires should be 10 or 100 atoms in diameter, and the circuits should be a few thousand angstroms across. [...] There is plenty of room to make them smaller. There is nothing that I can see in the laws of physics that says the computer elements cannot be made enormously smaller than they are now.*

Molecules have been investigated as possible candidates to the building blocks of the post-CMOS era. The smaller dimensions and the electronic properties that characterize these systems (in particular, the possibility to withstand high current densities) have attracted much interest in the scientific community.

The idea of molecules as electronic component is more than 35 years old, with the seminal work of Ari Aviram and Mark Ratner[3] that described the possibility of use a molecule as one of the most fundamental electronic circuit device, the rectifier (or *diode*). Over the years, the design and development of electronic devices exploiting molecular functionalities (field known as *Molecular Electronics*) has been a difficult and appealing task for chemist, physicist

and engineers. In particular, the realization of molecule-based devices has faced the problem of the reliability and reproducibility, which are not yet completely resolved. The introduction of Scanning Tunneling Microscope (STM) and Mechanically Controllable Break Junction (MCBJ) techniques have made enormous advances, towards the realizations of devices with reproducible current/voltage characteristics and room temperature operation. The first measure of current/voltage characteristics of molecules sandwiched between metal electrodes has been reported by Reed *et al.*,[4] using benzene-1,4-dithiolate connected between stable metallic Gold contacts and the MCBJ technique for the realization of the metal/molecule junction. Current-voltage I(V) and conductance G(V) measurements showed reproducible characteristic features of stepped conductance and an I/V characteristics which had a ~ 0.7 V gap before the current started to flow in the molecular junction. An interpretation of the observed gap is due to the mismatch between the contact Fermi level and the benzene-benzene-1,4-dithiolate LUMO.

Parallel to the experimental advancing in measuring conductance and I/V characteristics of single molecules, great effort was devoted in understanding the laws behind transport at the meso- and nanoscale. This effort has lead to the formulation of theories describing more and more accurately the fundamental processes at the heart of nanoscale transport. These are investigated from first principles by using numerical simulations, which are often quite expensive in terms of computational time and resources. Consequently, such computational approaches depend on efficient numerical algorithms in order to be successful. To calculate conduction properties of molecules (or, more in general, nanoscale junctions), one approach is based on Density Functional Theory (DFT) (which is used to calculate electronic properties of the system) coupled with Non-Equilibrium Green's Function Method (NEGF) and Landauer-Büttiker theory. This particular approach is by far the most widely used method, and, with some appropriate approximations and optimized algorithms, NEGF-DFT has become a cost-effective first-principles method and has been used to reproduce particular molec-

ular transport features and also to understand the physics behind the transport process, even if sometimes discrepancies between computed and experimental data arises. There is, then, still much work to do in the field of computational molecular electronics, in the direction of a better description of the interaction between molecules and electrodes, a better description of the physics behind electron transport mechanism and therefore better experimental/computational data agreement, and also in view of cutting the computational costs relating to the evaluation of quantity involved in the current/voltage characteristics of molecules and nanojunctions in general.

The main work done in this Thesis concerns electronic transport through molecules, aiming at the definition of a simple, and computationally low-cost procedure to calculate transmission functions and current/voltage characteristics of systems at the molecular scale sandwiched between two semi-infinite electrodes, a setup usually present in molecular electronics experiments. The action of an external bias voltage is done without the need of the standard self-consistent procedure employed in most of the commercial codes dealing with quantum transport. Application of the procedure to the calculation of electronic transport properties for molecular species with a potential technological interest in integrated circuit design will be discussed, beginning with those that show a diode-like behaviour, trying to explain the underlying mechanism of molecular rectification.

The second Chapter will present a brief introduction of the subject, and how quantum transport is becoming more and more important since the main electronic devices found in integrated circuits (for example, transistors) are becoming smaller and smaller, up to the length scales where quantum phenomena are directly affecting transport properties and the overall behaviour of the devices.

The third Chapter will outline one of the possible theoretical frameworks used to tackle the problem, that is the Landauer-Büttiker model coupled with Non-Equilibrium Green's Function (NEGF) method. This method requires a complex self-consistent procedure, which involves the calculation of the Green's function and the elec-

tric field in the central region. On top of that, the entire procedure should be repeated for every voltage applied. We therefore developed a new simplified method, implemented in the domestic code called FOXY, whose aim is to reduce the computational cost of calculations, avoiding self-consistent schemes, and focusing on the response of the contacted molecule to the voltage bias rather than to the details of the contact.

The fourth Chapter is about the calibration and application of the FOXY code to molecular species of interest. After the calibration, we were able to study in detail molecular rectifiers and switches proposed in the literature. The first example is a device which has been experimentally measured by Weber *et al.*[5] We have been able to reproduce the experimental I/V curves and to explain the underlying rectification mechanism. We then studied binuclear transition metal complexes of the VIII group, where the metallic moieties are bridged by aromatic ligands, and we found that they do not present particularly pronounced rectifying behaviour, with rectification ratios in the order of ~ 2 in the best cases. However, the introduction of electron-withdrawing substituents increased and stabilized the rectification ratios over a broader range of voltages, still being far from values which can be useful in real electronic applications. The third class of devices consist in two molecular switches based on a slightly modified diarylethene moiety, which changes from an high conductive state to a low one by the means of an external optical stimulus. We were able to reproduce experimental ON and OFF currents for both switches, and we were able to explain the switching effect by means of transmission function and orbital analysis.

The fifth Chapter concludes this Thesis, summarizing the key findings.

The entire work was done under the supervision of Prof. Vincenzo Barone, Prof. Ivo Cacelli and Dr. Alessandr Ferretti, at the *Istituto di Chimica dei Composti Organo-Metallici* (ICCOM), of the *Consiglio Nazionale delle Ricerche* (CNR), in Pisa.

Chapter 2

Molecular Electronics

Historians tell us that in ancient times musicians, actors and painters went from court to court following the most interesting jobs by the powerful Lords. From here the common and famous expression: what is the state of the art now?

Matteo Piccardo

In present-day electronic circuits, data processing, storage and transmission are obtained using a specific class of devices based on MOSFET (Metal-Oxide -Semiconductor Field-Effect Transistor) technology, exploiting the interplay of metal/oxide/semiconductor interfaces. The most important device in modern integrated circuits (IC), designed with this technology, is the *transistor*.

Between the different types of semiconductor devices proposed in the past, only the MOSFET emerged as a viable solution to the many requirements that a semiconductor device needs to have, and they were the only class of devices capable of an increase of the per-

formances with a constant dimension reduction, following a strict scaling law.

Fig. 2.1 shows the basic structure of a MOSFET. There are two P-N junctions that are called *source* and *drain* respectively. The drain supplies the device with electrons, while the source drags them away from the central channel region (an initially non-conducting region between the source and drain very close to the silicon surface). The name Field-Effect Transistor (or FET) refers to the fact that the *gate* (the third contact, above the central channel) turns the transistor "on" and "off" with an electric field through the oxide: when a positive voltage is applied to the gate, electrons from the silicon bulk are attracted to the transistor channel. When the gate voltage becomes sufficiently positively charged, enough electrons are pulled into the channel from the bulk to establish a charged path between the source and the drain. Electrons flow across the transistor channel, and the voltage-controlled switch is conducting. If a 0 or a very small voltage is placed on the gate, no electrons (or at least very few) are attracted to the channel. The source and drain are disconnected, no current flows across the channel, and the switch is not conducting.

A transistor is a device that presents a high input resistance to the signal source, drawing little input power, and a low resistance to the output circuit, capable of supplying a large current to drive the circuit load. Fig. 2.1 also shows the MOSFET IV characteristics. Depending on the gate voltage, the MOSFET can be "of" (conducting only a very small off-state leakage current, I_{off}) or "on" (conducting a large on-state current, I_{on}).

Transistors are traditionally been made from bulk materials. This means that in order to increase performance gains and complexity, as the famous Moore's Law[1] (the historical integrated circuit scaling cadence and reduction of cost/function law) predicts, their size should shrink following the rules of device scaling. As the structure of the device decreases, the transistor building process must be controlled to a precision of a few atoms for the devices to work properly. This "bulk approach" (also called "top-down" approach),

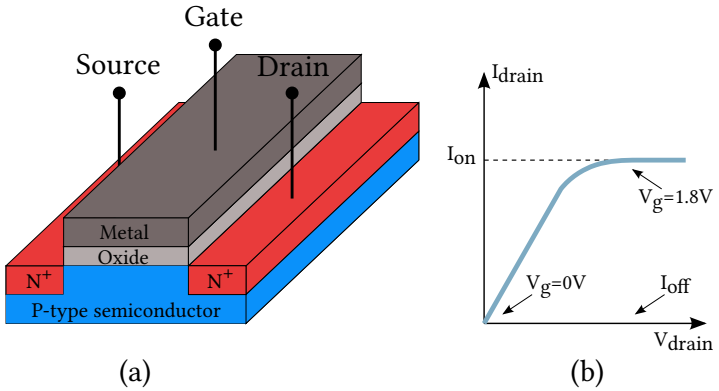

Figure 2.1: (a): basic field-effect transistor (MOSFET) structure; (b): ideal MOSFET I/V characteristics

in which devices are usually built from lithographic methods, is becoming more and more demanding and expensive, other than slowly approaching the inherent limitations on the control level of the building process. In order to circumvent the problem, one can think of new paradigms for systems architecture that are capable of meeting the same requirements that the MOSFET device are capable now (and will be capable up to the near future) still with a scaling of the dimension of the device itself and a reduction of the power usage, sticking with the "top-down" approach outlined above.

It is then possible to think of radically change the approach in building nanodevices: instead of creating structures by removing or applying material after a pattern scaffold, the device is ideally built in a chemistry lab, atom by atom. In this way a large number of copies are made simultaneously while the composition of the systems are controlled down to the last atom. This approach is called "bottom-up".

It is clear that molecules are well suited to become focal element of a new class of devices built by employing "bottom-up approaches".

The smaller dimensions and the electronic properties that characterize these systems make molecules good candidates to become basic blocks for future electronics. "Molecular Electronics" is, therefore, the discipline that aims to reproduce conventional electronic circuit elements with molecules, hoping to reach performances comparable to the present-day Silicon-based devices. Molecular electronics is conceptually different from conventional solid state semiconductor electronics. It allows chemical engineering of organic molecules with their physical and electronic properties tailored by synthetic methods, bringing a new dimension in design flexibility that does not exist in typical inorganic electronic materials. In contrast with the typical "top-dow" approach in the fabrication of solid-state devices, molecules are synthesized from the bottom (bottom-up approach), which means that small structures can be fabricated, starting from the bottom, from the molecular or single device level. It in principle allows a very precise positioning of collections of atoms or molecules with specific functionalities. Also, chemical synthesis can, in principle, make large quantities of molecular devices with relative low cost (lesser than the one for modern micro- or nano-lithography currently used for semiconductor devices fabrication) and prepare molecules with structures possessing desired electronic configurations and attach/interconnect them into an electronic circuit using surface attachment techniques like self-assembly.[6] Self-assembly is a phenomenon in which atoms and molecules or group of molecules arrange themselves in ordered patterns without external intervention.

The design and development of electronic devices exploiting molecular functionalities has been a challenging task for chemists, physicists and engineers for the last few decades.[7–10] Although several conceptual and technological problems still make the realization of working molecular-based devices a far off goal, the fascinating diversity of molecules, and thus the possibility of designing and synthesizing molecular species purposely tailored for specific functions, is sufficient to justify the intense effort spent in the field. For example, negative differential resistance devices[4] and rectifiers[11] have already

been demonstrated at the molecular level, as well as fully functional transistors[12] , memories and logic gates.[13,14]

Transport through molecule presents peculiar features in general different from the one seen in standard metals or semiconductors. The main reason is that with molecules we don't work with Fermi surfaces but with a defined number of discrete energy levels. The nature and lineup of the molecular levels with the Fermi energy of the electrodes determine most of the transport properties. In absence of any coupling between the molecule and the continuum of states provided by the electrodes, both the energy levels of the molecule and the Fermi level of the electrodes will align with a common vacuum level. In this case the system is characterised by the work function (WF) of the electrodes and both the ionisation potential (IP) and the electron affinity (EA) of the molecule. The only way the molecule and the electrode can exchange electrons is to provide an external energy comparable to either $IP - WF$ or $WF - EA$.

In contrast, the interaction between the molecular levels and the metallic contacts has the effect of broadening and shifting the molecular levels. In the extreme limit of large coupling, extended states spanning through the entire system (electrode plus molecule) can occur and the molecular device will behave as a good conductor. The effect of an external bias is to shift the electrochemical potentials of the electrodes relative to each other by eV, with V the external voltage and e the electron charge. Roughly speaking, a current starts to flow if some broadened occupied or virtual levels are inside the formed bias window.

There are several techniques available to date for manipulating and contacting single molecules to macroscopic electrodes in order to investigate their functionalities. However, the computational modelling and theoretical understanding of the various processes still suffers from several difficulties which often do not allow a comparison between experimental and computational data, due to discrepancies of one or two orders of magnitude.[15,16] Charge transport in single molecules is indeed a very complex problem and results from the interplay of several basic physical effects. Any simplification of

the problem without loosing essential physical content is therefore a very hard task.

2.1 Molecular requirements for electronic conduction

The two basic requirements for electronic conduction in a generic material are:

- a continuous system of a large number of strongly interacting atomic orbitals leading to the formation of electronic band structures;
- the presence of an insufficient number of electrons to fill these bands.

In inorganic semiconductors and metals, the atomic orbitals of each atom in the crystalline structure of the material overlap, creating a number of continuous energy bands, and the electrons, initially pertained to each atom, are delocalized across the entire structure. The strength of interaction between the overlapping orbitals determines the extent of delocalization, giving rise to the bandwidth. Likewise, in a molecule, a set of overlapping delocalized electronic states across the entire molecule is necessary for electronic conduction.

Conjugation, in molecular electronics, is an important property that is usually sought, in order to have molecules capable of providing a substantial current (at least in the order of nA) in output. π-conjugated molecules contain systems of alternating single and double bonds. sp_2 or sp_3 hybridisation of parallel p atomic orbitals leads to the formation of diffuse bonding orbitals in the plane of the sigma bond (a double bond). Multiple equivalent structures exist depending on which permutation of alternating bonds are considered. These contributing structures can mix together forming a hybrid structure at a lower energy due to the increased delocalization of

the electrons. Conjugation within aromatic structures leads to high stability and planarity, the ring of connected p-orbitals from the sp_2 hybrid carbons forming a shared volume of electron density above and below the plane of the ring.

In conjugated molecular electronic materials, the charge carriers occupy these extended molecular orbitals. The diffuse nature of the conjugated π orbitals results in sufficient overlap for charge transfer. Also, these extended orbitals easily overlap with electrodes' states, resulting in orbitals delocalized over all the extended structure (electrodes plus molecule). Large regions of delocalized charge carrying orbitals mean that electrons can cross a large region of space in fewer hops. These hops are the rate limiting step that decide macroscopic electron mobilities. Larger regions of charge delocalisation, and greater electronic wavefunction overlap between systems would be expected to lead to larger mobilities.

The performance of molecular electronic materials is highly dependent on the purity of the material produced. Defects and contamination tends to form charge traps which severely degrades performance. The performance is also highly dependent on processing conditions used by the device fabricator. It can take many years of effort working on improving a chemical synthesis, and simultaneously optimising devices to know whether a material is intrinsically better than the state of the art.

Apart from consideration about conjugation, for a molecule to be useful for electronic applications, it must be addressable. This mean that it must remain in the physical location in space where it is placed. There are two important concerns in this regard. First, it is presently somewhat difficult to position molecules exactly where they are desired. Certainly there are examples of both atomic and single molecular positioning, however, these examples have not been focused at limiting the long-term propensity of the molecule to diffuse. Also, a primary consideration of any molecular electronic candidate must be that of chemical stability. It is important to understand the long-term stability of any molecular electronics component under a wide variety of conditions. If a molecule tends to decom-

pose when exposed to elevated temperatures, then it is not a good candidate for use in a molecular electronic device. Similarly, the species must be inert with regards to other molecules of the same type, a requirement that is particularly important in devices involving charge-storage or redox-active molecules. Species that show poor insulation from each other would tend to exchange stored electrons, scrambling any data represented by the storage of those electrons. Conversely, a molecule which shows an irreversible electron transfer would not be a good candidate for any sort of molecular electronic device as the point of electronics is to utilize reversible charge transfer from one element to the next. Finally, describing a molecule doing some useful function does not automatically make it a molecular electronic device. There must be a way to interact with the component, both on a microscopic level and through input from the macroscopic world. Thus it is important to consider how a molecular electronic device can be "wired up". It must be able to exchange information, or transfer states to other molecular electronic devices, or it must be able to interface with the components in the system that are not nanoscopic. These requirements present challenges which are just beginning to be addressed.

2.2 Computational strategies for molecular devices

From the molecular electronics point of view, the goal is to determine the I/V characteristic of a device that mainly consists in a central molecular region coupled with two semi-infinite metallic electrodes which are under the influence of an external bias. This is made with the aim of understanding and optimizing its characteristics and features. Before describing in detail the quantum-mechanical techniques used for this task, it is necessary to find a simple model that describes the underlying physics of a metal/molecule junction.

Electronic transport through molecular devices significantly differs from the one through macroscopic heterostructures. In the latter, the effective mass approximation is, in general, satisfactory, due to the periodicity of the overall structure and the great mean free path length (which is the average distance travelled by a moving electrons without experiencing scattering events) for the electron that travel across the system. On the contrary, in a molecular device the electrons interact with a relatively small set of atoms, whose spatial position is important. Therefore, the effective mass approach fails to describe correctly the system, and the electronic structure of the molecular device should be explicitly taken into account. Frequently, Density Functional Theory (DFT) is used in order to calculate electronic properties for these kind of systems.[17,18] DFT theory states that the entire problem of finding the many-body wavefunction is reduced to that of calculating the equilibrium charge density $\rho(\mathbf{r})$, via the Hohenberg-Kohn theorems, that state that, given the solution of the Schrödinger equation, and given the ground state (assumed non-degenerate), the external potential, and hence the total energy, is a unique functional of the electron density ρ, and the density that minimises the total energy is the exact ground state density. Also, the Kohn-Sham method maps the entire problem onto a non-interacting one, introducing a system of non-interacting electrons that generates the same electron density as the interacting one. So, thanks to the Kohn-Sham method, the entire DFT problem can be formulated as a ground-state, single-particle problem, and energies and eigenvalues can be calculated. However, conventional DFT methods are best suited for systems in which the total number of particles is conserved. Also, DFT presents some well known problems that could lead to discrepancies between computed and measured data. For instance, one of the most used theories for electronic transport through molecules (described in detail in the next chapter), after reducing the overall open, infinite and out of equilibrium problem to a closed and finite one, requires an accurate estimate of the energy levels, both occupied and virtual. The choice of DFT for electronic structure calculation might then introduce uncertainties or even lead

to fake results.

Lang *et al.*[19,20] proposed a method for which, using a jellium model for the metallic electrodes in a electrode/molecule/electrode system, it is possible to map the Kohn-Sham equation of the system onto the Lippman-Schwinger scattering equation, and then solve the equations in a self-consistent way for the scattering states. Then the current will be calculated summing up each scattering state contribution to electron flow, with an approach similar to the one used in the Landauer-Büttiker theory (described in the next chapter). This model is simple, but limited: for example, it cannot correctly analyse strongly directional bonds as it occurs in semiconductors and in transition metal compounds. This results in a lack of evaluation of charge transfer between electrodes and the central molecule, which is a very important quantity in transport problems.

Another possibility is to implement Landauer-Büttiker transport theory directly.[7,8,21] In this model, electrons transmit from one electrode to the other through the central scattering region by a series of scattering events which limit the transmission probability of each electron (described by the *transmission function*). The net current is then obtained integrating over the energy range defined by the Fermi level of the system and the applied bias, the transmission function. This theory poses its foundations on a series of approximations, one of which is that electron interactions have been included only at the mean-field level. In fact, DFT is usually employed for the calculations of the electronic properties of the system. This is quite a strong approximation, especially in nanojunctions, where large current densities are common. In order to calculate the transmission function, a Non-Equilibrium Green's Function (NEGF) specific formulation that regards steady-state transport is used. In general, this technique allows the calculation of coherent transport properties in a complete self-consistent way. In order to properly treat charge transfer phenomena, electrodes and central region are treated on the same footing, and some part of the electrodes (few atoms to some layers of atoms) should be included in the central scattering region, forming an "extended molecule".

It is also possible to implement a full Non Equilibrium Green's Function (NEGF) method, also known as the Keldysh formalism,[22,23] which allows us, at least in principle, to solve the time-dependent Schrödinger equation for an interacting many-body system exactly, from which one can, in principle, calculate the time-dependent current. This is done by solving equations of motion for specific time-dependent Greens functions, from which the physical properties of interest, such as the charge and current densities, can be obtained. Even this methodology is based on some assumptions: it applies only to closed systems (so it is necessary to find a way to effectively close an open problem such as the transport one), and it needs that the total Hamiltonian is described by an unperturbed Hamiltonian plus a perturbation switched on adiabatically at a certain time (the perturbation can be, for instance, an external field). Other than that, as in the Landauer-Büttiker method, in order to get the steady-state total current, it is necessary to introduce other approximations: for example we have to assume non-interacting electrons, but this time only in the leads. So, in essence, the Non Equilibrium Green's Function formalism for steady-state transport problems helps to deal with many-body interaction in the central region, not treating such interaction at the mean-field level, in order to get more information on the transport process. The method makes large use of the contour-ordered Keldysh Green's function:

$$G(\mathbf{r},t,\mathbf{r}',t') = -\frac{i}{\hbar}\langle T_c\left[\psi_H(\mathbf{r},t)\psi_H^\dagger(\mathbf{r}',t')\right]\rangle \tag{2.1}$$

where $\psi_H(\mathbf{r},t)$ is the field operators written in Heisemberg representation (with respect to the total perturbed Hamiltonian $\widehat{H}$) and T_c is the time-ordering operator. The theory also makes use of the lesser Green's functions $\widehat{G}^<$ (that stem from the general Keldysh Green's function definition) and of the Keldysh equation, which is just a way to express the equation of motion of the lesser Green's function in terms of self-energies (effective potential that represent the interaction of a single electron with all the other particles in the system). From that, it gives us a formula for calculating the total

current by means of $\widehat{G}^{<}$ and broadening (quantities that are related to self-energies, which in some way represent the broadening of the discrete central region levels):

$$I = \frac{ie}{\hbar}\int \mathrm{Tr}\Big\{ \left[\Gamma_L(E) - \Gamma_R(E)\right] G^{<}(E) + \\ + \left[f_L(E)\Gamma_L(E) - f_R(E)\Gamma_R(E)\right]\left[G^{+}(E) - G^{-}(E)\right] \Big\} \frac{dE}{2\pi} \tag{2.2}$$

Attempts have also been made to work directly with many-body wave-functions,[24] and the Green's function formalism, combined with the GW approximation[25,26] (where the self-energy is calculated to lowest order in the screened interaction W) is leaning towards overcoming the known problems related to the use of a mean-field theory for transport calculations.

As stated earlier, Landauer-NEGF method is based on the idea that the description of the electronic ground state at the DFT level is sufficient for describing the current flow through a channel, even if the system is not at equilibrium. This could lead to discrepancies between the computed data and the measured ones,[27,28] because it does not allow the inclusion of dynamical multi-state effects. Also, the most important quantities that define the transport properties of the system under study are computed with non-interacting Kohn-Sham excitation energies, which in general do not coincide with the true excitation energies. Standard NEGF-DFT theories also neglect the role of vibrational degrees of freedom, whose coupling to the electronic motion may indeed be relevant (e.g. molecular resistance) and is now also under active study. Excitation energies of interacting systems are accessible via time-dependent (TD) DFT.[29,30] In this theory, the time-dependent density of an interacting system moving in an external, time-dependent local potential can be calculated via a fictitious system of non-interacting electrons moving in a local, effective time-dependent potential. Therefore, this theory is in principle well suited for the treatment of non-equilibrium transport problems.[31–34] Time-dependent simulations of current-carrying molecular devices are required to describe the transient re-

sponse to an external perturbation. There is an increasing interest in time-dependent (TD) simulations of current-carrying molecular devices, from a variety of points of view.[32–42] In general, time-dependent approaches can address the problems related to the use of a ground-state steady-state theories (and, in particular, aim at a better *quantitatively* agreement with experiment), as well as underline the transient response of nanoscale junctions and better describe excited states (particularly useful if interested in the analysis of optical switches, where an external light pulse can variate the transmission properties of selected molecules). Usually, the whole treatment starts from the Liouville equation for the system:

$$\frac{\partial \widehat{\rho}}{\partial t} = \frac{1}{\imath\hbar}\left[\widehat{H}\left[\widehat{\rho}\right], \widehat{\rho}\right] \tag{2.3}$$

where $\widehat{\rho} = \widehat{\rho}(t)$ is the reduced one-electron density matrix and $\widehat{H}[\widehat{\rho}]$ is a generic one-electron Hamiltonian (such as the one produced by time-dependent density functional theory). In a TD-DFT picture, we are sure that, if the system is partitioned, then the total particle current between the regions computed from one-electron density matrix is formally exact.[36,43] Without something that guarantees a continual supply of electrons that have flown across the junction back into the starting electrode, the system would rapidly return in equilibrium. This is avoided by maintaining the charge imbalance, and hence the current, in the system by a driving term operating at the density matrix level:

$$\frac{\partial \widehat{\rho}}{\partial t} = \frac{1}{\imath\hbar}\left[\widehat{H}\left[\widehat{\rho}\right], \widehat{\rho}\right] - \Gamma\left(\widehat{\rho} - \widehat{\rho}_0\right) \tag{2.4}$$

where Γ here just represents the driving term which maintains the charge imbalance at the boundary of the transport region. Other approaches are based on the direct time propagation of the wavefunction. This approaches can be interesting because one can exploit the advanced computational methods that have been developed to solve the time-dependent Kohn-Sham equations. Even here, one

of the main challenges is the proper treatment of boundary conditions: one way to address this problem is to employ specific boundary potentials.[32,44,45] These potentials are typically local in space, purely imaginary, with negative imaginary part, they vanish inside the transport region and grow rapidly away from that region. The negative imaginary part will cause asymptotic damping of resonant eigenfunctions, preventing them to extend to infinity. Because these potential effectively absorb particles that would otherwise escape to infinity, they are known as complex absorbing potentials (CAP). Another basic issue with time-dependent DFT approaches is that most exchange-correlation functionals have been derived under equilibrium conditions and their application to non-equilibrium problems should be analysed in more detail.

Chapter 3

Electron Transport in Nanostructures

One single advice should be given to those who want to leave their footprints, in Science or in Arts: if you are giving birth to a new theory or movement, make sure its name will sound good in German.

Nicola De Mitri

In order to address the transport problem at the nanoscale level, a full quantum-mechanical approach is needed. At the atomic level, classical description of physical systems gives way to quantum mechanics, and in some cases, special relativity, and when modelling atomic scale circuits, one must introduce a treatment in terms of wave functions and transmission probabilities, an aspect usually ignored in conventional electronic engineering. In classical theory, the

resistance of a material is defined by Ohm's Law:

$$V = RI \tag{3.1}$$

where V is the external voltage, R the resistance and I the current flowing in the system. Leaving the geometrical details of the sample in consideration apart, Eq.3.1 may also be written as:

$$\mathbf{E} = \rho \mathbf{j} \tag{3.2}$$

in which the *resistivity* ρ is defined as the proportionality constant between the field E applied to our system and the current density j. Inverting Eq.3.1, we get:

$$I = GV \tag{3.3}$$

where G is the *conductance*. We can easily see that, in this classical picture of the electrical properties of a system, there is a linear relation between the applied field and the generated current density: a variation of the field produce a variation in the current density which is proportional to the applied voltage by means of the resistivity.

Assuming an uniform conductor, with resistivity ρ, length l and cross-section S, we can calculate the constant voltage drop across the conductor as $V = El$, the total current then is $I = Sj$ and we can calculate the resistance of the system as:

$$R = \rho \frac{l}{S} \tag{3.4}$$

This classical relation states that, for Ohmic conductors, the resistance is proportional to the length of the conductor, and inversely proportional to the cross-section. So, in the classical model, it seems that, "playing" with the parameters, it is possible to indefinitely lower the value of the resistance.

As the precision of measuring instrument rose in time, and new techniques were exploited in order to fabricate smaller and smaller conductors, new experiments on conductance of mesoscopic and

nanoscopic conductors were performed. What emerged from the experiment was a different picture with respect to what was foreseeable from the classical description of conduction. The work of van Wees *et al.*[46] is the first example of experimental study on conductance of mesoscopic systems (in this case, conductance of quantum point contacts in the two-electron gas of high-mobility GaAs-AlGaAs heterostructures). The results showed clearly that the conductance was quantized in multiples of the fundamental quantity $e^2/\pi\hbar$. Therefore, the classical theory of conduction needed to be revisited in order to explain this novel quantum effect.

The typical setup, when dealing with nanoscopic electron transport problems, consists in a channel region (either a nanostructure, a solid state device, a monolayer of molecules or a single molecule) sandwiched between two metallic regions (electrodes, considered as semi-infinite due to the fact that their dimension is much bigger than the one of the channel). An external voltage is applied to the electrodes, and a current starts to flow in the channel region. It is clear that the system is intrinsically open (due to the external voltages), semi-infinite (due to the presence of the electrodes), and out of equilibrium (in order to ensure a current flow, the voltages applied to the electrodes must be different). It is then clear that approximations are needed in order to treat the problem from a computational point of view. The main idea is, therefore, to calculate the transmission probability that an electron can tunnel across the junction, from one electrode to the other, under the influence of an external bias that maintains the entire (open, semi-infinite) system out of equilibrium.

One of the possible way to address this problem is to start with a good description of the central channel region (by a suitable Hamiltonian) and then use the Green's function method, coupled with the Landauer-Büttiker model for quantum transport in mesoscopic or nanoscopic systems.[47–50]

3.1 Landauer-Büttiker model

The Landauer formalism[21] is a simple phenomenological one-electron model which dose not take into account the inelastic processes or the electron-electron interaction, but still it has been very powerful to explain several mesoscopic phenomena, and it also helps to understand the nature of conductance at atomic level.

The whole method poses its foundation on a number of approximations regarding the overall problem. The first assumption here is that a unique steady-state solution for the current is reached. Here, in fact, we do not work with time-dependent densities, but with time-independent $\rho(\boldsymbol{r})$, as if we have effectively reached a stationary solution (*if it exists*, which is, in theory, not assured) after enough time. Once the problem has been made ideally stationary, the role of the electrodes (or *reservoirs*) is to continually prepare electrons that move across the junction, without changing in time. They also have to be "reflectionless", that is, the electrons can enter them from the conductor without suffering reflections. We then assume to switch from an open problem to a closed one via a set of boundary conditions that are usually called *scattering boundary conditions*, with electrons that arrive without scattering from the electrodes, scatter through the junction and then move away from the junction, without further scattering. It is also required by the Landauer-Büttiker method to treat the many-body problem with a ground-state mean-field theory, even if the system is not in its ground state and there are, usually, complicated many-body interactions. Other than that, the theory assumes that every transmission channel is independent, or better assumes that the system has somehow evolved in a totally incoherent (independent) set of (single-particle) channels, populated with a Fermi-Dirac statistics. All of these are rather strict approximation that we have to introduce in order to solve the problem, and neither of them are guaranteed to be satisfied in a nanojunction. So the whole theory, soon to be outlined, should be used with particular care.

As a first step, let us consider the left and right reservoirs, each at a specific electrochemical potential μ_L and μ_R, respectively, and defined by Hamiltonians H_L and H_R. They can be viewed as ideal blocks of conducting material with a constant transversal confining potential along its axis. The quantum mechanical solution for the wavefunction of such systems gives electron states, which are plane waves along the wire axis and standing waves in the transversal direction. Let us also suppose that the current flows in the z direction. The energy dispersion relation for the electrodes is (see for example Fig. 3.1):

$$E_\alpha(k) = \epsilon_\alpha + \frac{\hbar^2 k^2}{2m} \tag{3.5}$$

where k is the wave vector in the axis direction and ϵ_α is the energy of the α-th transverse wave function. Also, given an energy E, the number of transverse modes at that energy is:

$$N_C(E) = \sum_\alpha \Theta(E - \epsilon_\alpha) \tag{3.6}$$

with Θ the Heaviside step function. Now that we have defined the solution at the boundaries, we need to find the general solution for the whole system, which is defined by single-particle Hamiltonian H_S. This Hamiltonian satisfies the asymptotic conditions:

$$\lim_{z\to-\infty} H_S = H_L \tag{3.7}$$

$$\lim_{z\to+\infty} H_S = H_R \tag{3.8}$$

So, the eigensolutions of H_S should asymptotically merge with the ones obtained for the electrodes (plane waves along the wire axis and standing waves in the transversal direction). We can now, as an example, take an electron coming from the left lead, with energy E_i and eigenstate $|\psi_{i,k_i}\rangle$ (with $\hbar k_i$ its momentum). This electron then experiences certain scattering events (whose nature is not important) due to the contact. Starting from a single wave, after the scattering process, in the right electrode this state will be a linear combination

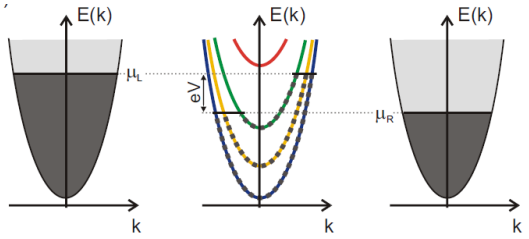

Figure 3.1: Energy dispersion and occupation of the states in the system. In the leads the quasi-continuous transversal modes are filled up to their chemical potential. Due to the small transversal dimension in the ballistic conductor only a few modes are occupied, and the $+k/-k$ states have different fillings (dark grey dotted line) depending on which electrode they arrive from.

of transmitted waves $|\psi_{f,k_f}\rangle$ (N_C^R represents the channels at energy E_i in the right lead):

$$|\Psi_{i,k_i}\rangle \longrightarrow \sum_{f=1}^{N_C^R} \mathfrak{T}_{if} |\psi_{f,k_f}\rangle \tag{3.9}$$

In the same way, after the scattering event we expect the solution in the left lead to be a combination of the incident wave and a sum of the reflected waves at the same energy E_i of the incoming wave:

$$|\Psi_{i,k_i}\rangle \longrightarrow |\psi_{i,k_i}\rangle + \sum_{f=1}^{N_C^L} \mathfrak{R}_{if} |\psi_{f,k_f}\rangle \tag{3.10}$$

Since we have assumed that we have reached a steady state, the current carried by the state $|\Psi_{i,k_i}\rangle$ cannot depend on the position, on our system, of the surface at which we evaluate it. We can then observe the current deep in the left lead or deep in the right lead.

For the left and right lead we have, respectively:

$$I_L(E_i) = I_i(E_i)\left(1 - \sum_{f=1}^{N_c^L} R_{if}(E_i)\right) \tag{3.11}$$

$$I_R(E_i) = I_i(E_i)\sum_{f=1}^{N_c^R} T_{if}(E_i) \tag{3.12}$$

where $I_L(E_i)$ and $I_R(E_i)$ are calculated from the general quantum-mechanical definition of the current density:

$$j = \frac{\hbar}{2mi}\left(\Psi^* \frac{d\Psi}{dz} - \frac{d\Psi^*}{dz}\Psi\right) \tag{3.13}$$

using $|\Psi_{i,k_i}\rangle$ as the current-carrying state. In the same way, we defined $I_i(E_i)$ and $I_f(E_i)$ as the current densities from single eigenstates $|\psi_{i,k_i}\rangle$ and $|\psi_{f,k_f}\rangle$ in coordinate representation which, after some algebraic steps, become:

$$I_i(E_i) = \frac{\hbar k_i}{mL_z} = \frac{v_i(k_i)}{L_z} \tag{3.14}$$

$$I_f(E_i) = \frac{\hbar k_f}{mL_z} = \frac{v_f(k_f)}{L_z} \tag{3.15}$$

with L_z the length of the central region. R_{if} and T_{if} represent the reflection and transmission probability for a wave (with momentum $\hbar k_i$) incident to the central region to be reflected back in the left lead (with momentum $\hbar k_f$ and same energy) and to be transmitted to the right lead (again, with momentum $\hbar k_f$ and same energy). They are defined by:

$$R_{if}(E_i) \equiv |\mathfrak{R}_{if}|^2 \frac{|I_f(E_i)|}{|I_i(E_i)|} \tag{3.16}$$

$$T_{if}(E_i) \equiv |\mathfrak{T}_{if}|^2 \frac{|I_f(E_i)|}{|I_i(E_i)|} \tag{3.17}$$

which, due to the fact that we are postulating the existence of a steady state, have the property:

$$\sum_{f=1}^{N_c^R} T_{if}(E_i) + \sum_{f=1}^{N_c^L} R_{if}(E_i) = 1 \tag{3.18}$$

Note that the entire theory described up to now can be rewritten starting from a wave coming from the right lead, and the results do not change. Also, due to time-reversal symmetry, the indexes in T_{if} and R_{if} are interchangeable.

To calculate the total current, we must sum over all the transmitted and reflected waves. The density of states *per* spin for a momentum $\hbar k_i$ is:

$$D_i(E_i) == \frac{L_z}{2\pi\hbar v_i(k_i)} \tag{3.19}$$

the voltage V applied to the system causes, due to the assumptions initially made, a shift in the Fermi levels of the electrode by the relation $eV = \mu_L - \mu_R$, the electrons in the electrodes follow a Fermi-Dirac distribution at the electrochemical potentials $\mu_{L,R}$. The total current is then:

$$\begin{aligned} I \quad = \quad & 2e \int \Bigg\{ f_L(E) \sum_{i=1}^{N_c^L} \sum_{f=1}^{N_c^R} D_i(E_i) I_i(E_i) T_{if}(E_i) \\ & - f_R(E) \sum_{i=1}^{N_c^R} D_i(E_i) I_i(E_i) \left[1 - \sum_{f=1}^{N_c^R} R_{if}(E_i) \right] \Bigg\} dE \end{aligned} \tag{3.20}$$

Defining T_{LR} and T_{RL} as:

$$T_{LR} = \sum_{i=1}^{N_c^L} \sum_{f=1}^{N_c^R} T_{if}(E_i) \tag{3.21}$$

$$T_{RL} = \sum_{i=1}^{N_c^R} \sum_{f=1}^{N_c^L} T_{if}(E_i) \tag{3.22}$$

and, considering that the particle flux must be conserved:

$$T_{RL}(E) = T_{LR}(E) = T(E) \tag{3.23}$$

we finally get the expression for the total current in the Landauer Büttiker picture:

$$I(V) = \frac{2e}{h} \int_{-\infty}^{+\infty} [f_L(E) - f_R(E)]\, T(E) dE \tag{3.24}$$

3.2 Transmission function evaluation

According to the Landauer-Büttiker model, described in the previous Section, the net current flowing across a junction sandwiched between two metallic, semi-infinite contacts with electrochemical potentials $\mu_{L(R)}$ (L=left, R=right), as pictured in Fig. 3.2 can be expressed as:

$$I(V) = \frac{2e}{h} \int_{-\infty}^{+\infty} T(E,V)\, [f_L(E) - f_R(E)]\, dE \tag{3.25}$$

where f_L, f_R are the Fermi distribution for the left and right electrodes*, V is the external bias and $T(E,V)$ is the transmission function.

Eq.3.25 is usually written in a simplified formula, in which the Fermi statistic is taken just as a step function:

$$I(V) = \frac{2e}{h} \int_{\mu_L}^{\mu_R} T(E,V) dE \tag{3.26}$$

where $\mu_L = \varepsilon_f - V/2$, $\mu_R = \varepsilon_f + V/2$, $eV = (\mu_L - \mu_R)$ and ε_F is the Fermi energy of the entire system.

*Fermi-Dirac statistics for the left and right electrodes: $f_{L(R)} = \frac{1}{\exp(E - \mu_{L(R)}/k_B t) + 1}$

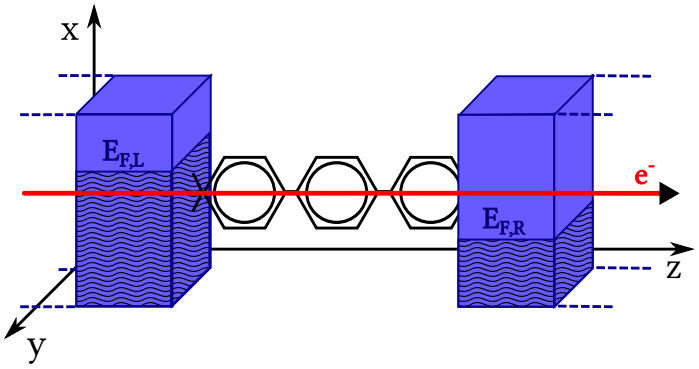

Figure 3.2: Schematic representation of the transport problem: two reservoirs at thermal equilibrium with a Fermi level ε_F are coupled to a central (confined) region. Upon an external bias applied to the electrodes, electrons start to flow.

To define a proper expression for the transmission function, it is necessary to start from the whole open system and divide it into three regions: L and R represent the two semi-infinite contacts, and C represents the channel region, sandwiched between the contacts. If we call $\hat{H}_S$ the Hamiltonian of the whole system, we could partition it in the three regions defined above, and assume that L and C are coupled by some potential $(\widehat{V}_{LC} + \widehat{V}_{LC}^{\dagger})$, while regions C and R, by a potential $(\widehat{V}_{CR} + \widehat{V}_{CR}^{\dagger})$, with $\widehat{V}_{LC}$ and $\widehat{V}_{CR}$ interaction operators. It is also assumed that L and R are decoupled[†], which means $VLR = VRL = 0$.

The isolated leads are described by the Hamiltonians $\widehat{H}_L$ and $\widehat{H}_R$, and it is possible to associate them with a Green's function ($\widehat{G}_L$

[†]This means that there is no direct tunnel between the electrodes

and $\widehat{G}_R$), according to

$$\widehat{G}(z) = \frac{\widehat{I}}{(z - \widehat{H})} \tag{3.27}$$

where z is a complex variable, $\widehat{I}$ is the identity and $\widehat{H}$ represents a generic Hamiltonian.

With these partitions in mind, it is possible to rewrite the total Hamiltonian as:

$$\begin{bmatrix} \widehat{H}_L & \widehat{V}_{LC} & 0 \\ \widehat{V}_{LC}^{\dagger} & \widehat{H}_C & \widehat{V}_{CR}^{\dagger} \\ 0 & \widehat{V}_{CR} & \widehat{H}_R \end{bmatrix} \begin{bmatrix} |\varphi_L\rangle \\ |\varphi_C\rangle \\ |\varphi_R\rangle \end{bmatrix} = E \begin{bmatrix} |\varphi_L\rangle \\ |\varphi_C\rangle \\ |\varphi_R\rangle \end{bmatrix} \tag{3.28}$$

where the φs are the single-particle wave functions associated to the three regions. Solving Eq.3.28 gives:

$$\widehat{H}_L|\varphi_L\rangle + \widehat{V}_{LC}|\varphi_C\rangle = E|\varphi_L\rangle \tag{3.29}$$

$$\widehat{V}_{LC}^{\dagger}|\varphi_L\rangle + \widehat{H}_C|\varphi_C\rangle + \widehat{V}_{CR}^{\dagger}|\varphi_R\rangle = E|\varphi_C\rangle \tag{3.30}$$

$$\widehat{V}_{CR}|\varphi_C\rangle + \widehat{H}_R|\varphi_R\rangle = E|\varphi_R\rangle \tag{3.31}$$

Rearranging the equations, it is possible to define φ_L and φ_R in terms of the Green's function of the left and the right contact:

$$|\varphi_L\rangle = \widehat{G}_L(z)\widehat{V}_{LC}|\varphi_C\rangle \tag{3.32}$$

$$|\varphi_R\rangle = \widehat{G}_R(z)\widehat{V}_{CR}|\varphi_C\rangle \tag{3.33}$$

Now, simply substituting Eq.3.32 and Eq.3.33 in Eq.3.30, we can express the new eigenstates of the channel region in the presence of the contacts:

$$\left[E - \widehat{H}_C - \widehat{V}_{LC}^{\dagger}\widehat{G}_L\widehat{V}_{LC} - \widehat{V}_{CR}^{\dagger}\widehat{G}_R\widehat{V}_{CR}\right]|\varphi_C\rangle = 0 \tag{3.34}$$

We define the *self-energy* operators for the left and right electrodes as:

$$\widehat{\Sigma}_L(z) = \widehat{V}_{LC}^{\dagger}\widehat{G}_L\widehat{V}_{LC} \tag{3.35}$$

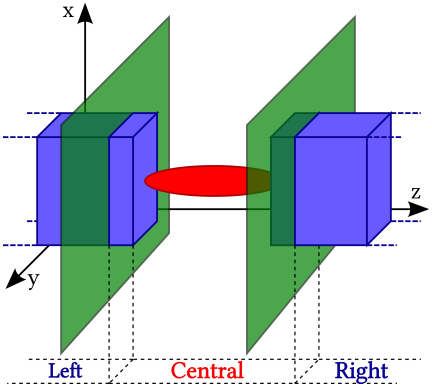

Figure 3.3: Regions in which the system is divided, as in 3.28. The proper central region (Channel) is the nanojunction plus part of the electrode. "Left" and "Right" are the parts which describe the true semi-infinite electrodes.

$$\widehat{\Sigma}_R(z) = \widehat{V}_{CR}^{\dagger}\widehat{G}_R\widehat{V}_{CR} \tag{3.36}$$

These terms (that depend also on the external bias V through the terms $\widehat{V}_{LC}$ and $\widehat{V}_{CR}$) represent an "effective" potential added to the Hamiltonian of the central region to take account of the interactions between semi-infinite contacts and the channel, and to switch between an open problem (due to the presence of the semi-infinite leads) to a closed one. Note that these terms are not Hermitian, so the eigenvalues $|\varphi_C\rangle$ are not real any more: since the eigenvalue spectrum of $\widehat{H}_L$ and $\widehat{H}_R$ is continuous, the discrete states ε_k of the channel broaden into resonances peaked around their corresponding eigenvalue, their starting energy is therefore shifted (or renormalized) by the presence of the electrodes, and the electrons acquire a finite lifetime to scatter from the channel into one of the electrodes, due to the broadening effect mentioned before. We can, in fact, consider an "effective" Hamiltonian $\widehat{H}_{eff} = \widehat{H}_C + \widehat{\Sigma}_L + \widehat{\Sigma}_R$, whose

eigenstates can be written as:

$$\left[\widehat{H}_C + \widehat{\Sigma}_L + \widehat{\Sigma}_R\right] |\Psi_i\rangle = \epsilon_i |\Psi_i\rangle \tag{3.37}$$

whose eigenvalues are, as said before, complex:

$$\epsilon_i = \epsilon_{i,0} - \Delta_i - i\left(\frac{\gamma_i}{2}\right) \tag{3.38}$$

Here, $\epsilon_{i,0}$ is the eigenenergy of the isolated conductor described by $\widehat{H}_C$. The time dependence of an eigenstate of $\widehat{H}_{eff}$ has the form:

$$\exp\left[-i\frac{\epsilon_i t}{\hbar}\right] \longrightarrow \exp\left[-i\frac{(\epsilon_{i,0} - \Delta_i)\, t}{\hbar}\right] \exp\left[-\frac{\gamma_i t}{\hbar}\right] \tag{3.39}$$

Δ_i represents the shift in energy due to the modification of the dynamics of an electron inside the conductor by the interaction with the leads. On the other hand, the imaginary part of the energy, γ_i, reflects the fact that an electron injected anywhere in the conductor will eventually disappear through one of the leads stretching out to infinity. Taking the squared magnitude of the wavefunction we obtain the probability:

$$|\Psi_i|^2 \exp\left[-\frac{2\gamma_i t}{\hbar}\right] \tag{3.40}$$

The quantity $2\hbar/\gamma_i$ this represents the *lifetime*, or the average time an electron remains in the state i before it escapes out into the leads. If the Hamiltonian would have been Hermitian, the lifetime would have been infinite.

Both Eq.3.35 and Eq.3.36 depend on the complex variable $z = E \pm i\delta$ (with δ as a positive infinitesimal constant). These equations, in fact, define two self-energy operators. We are interested only in the one depending on $z = E + i\delta$, or the *retarded* self-energy operator since, roughly speaking, the retarded solution (and the retarded Green's function to it related) is associated to the idea of an excitation which gives rise to "outgoing" travelling waves from the

excitation itself (the excitation being the interaction potential and the wave travelling in the positive z direction the "outgoing" wave from this excitation):

$$\widehat{\Sigma}_{L(R)}(z) = \widehat{\Sigma}_{L(R)}(E + i\varepsilon) \tag{3.41}$$

Now it is possible to recast Eq.3.34 as:

$$\left[E - \widehat{H}_C - \widehat{\Sigma}_L(E) - \widehat{\Sigma}_R(E)\right] |\varphi_C\rangle = 0 \tag{3.42}$$

and it is also possible to associate a retarded Green's function to this differential matrix equation:

$$\widehat{G}(E) = \frac{\widehat{I}}{E - \widehat{H}_C - \widehat{\Sigma}_L(E) - \widehat{\Sigma}_R(E)} \tag{3.43}$$

Given the self-energy operators, it is easy to define also the *broadening* matrices as the imaginary part of the self-energy operators, which are related to the broadening of the eigenstates:

$$\widehat{\Gamma}_{L(R)}(E) = i\left[\widehat{\Sigma}_{L(R)}(E) - \widehat{\Sigma}^{\dagger}_{L(R)}(E)\right] \tag{3.44}$$

In order to calculate the current, the only thing missing is an expression for the transmission function. This problem can be resolved relating all the theory explained above to scattering theory. The straightforward relation is to express scattered wave functions by means of the Lippman-Schwinger equation:

$$|\Psi^{+}_{i,k_i}\rangle = |\psi_{i,k_i}\rangle + \widehat{G}^{+}_0 \widehat{V} |\Psi^{+}_{i,k_i}\rangle \tag{3.45}$$

$$|\Psi^{-}_{i,k_i}\rangle = |\psi_{i,k_i}\rangle + \widehat{G}^{-}_0 \widehat{V} |\Psi^{-}_{i,k_i}\rangle \tag{3.46}$$

with $|\Psi^{+}_{i,k_i}\rangle$ representing a combination of an incident wave plus a linear combination of outgoing waves, and $|\Psi^{-}_{i,k_i}\rangle$ representing a

combination of an outgoing wave plus a linear combination of incoming waves. The scattering potential $\widehat{V}$ is simply (with $\widehat{V}_C$ the potential of the central region):

$$\widehat{V} = \widehat{V}_C + \widehat{V}_{LC} + \widehat{V}_{LC}^{\dagger} + \widehat{V}_{CR} + \widehat{V}_{CR}^{\dagger} \tag{3.47}$$

Given these equation, it is possible to rewrite the transmission and reflection probabilities, and in general, rewrite outgoing and incoming flux amplitudes. The relation between these flux amplitude is defined by the so-called $\mathbb{S}$ (scattering) matrix:

$$\mathbb{S} = \begin{bmatrix} r & t^{'} \\ t & r^{'} \end{bmatrix} \tag{3.48}$$

which connects the amplitudes of the outgoing and incoming waves in the nanojunction by the transmission and reflection matrices t and r. It is then possible to rewrite the total transmission coefficients in terms of the element of the $\mathbb{S}$ matrix:

$$T_{LR}(E) = T_{RL}(E) = \mathrm{Tr}\{tt^{'}\} = \mathrm{Tr}\{t^{'}t\} \tag{3.49}$$

Knowing the form of the Green's function, it is then possible to rewrite the transmission function (explicitly considering the dependence on the external bias) with known quantities as:

$$T(E,V) = \mathrm{Trace}\left[\widehat{\Gamma}_L(E,V)\widehat{G}(E,V)\widehat{\Gamma}_R(E,V)\widehat{G}^{\dagger}(E,V)\right] \tag{3.50}$$

Now, simply integrating Eq.3.50 as in Eq.3.26 we obtain the desired current.

It is clear that the picture here described focuses on the idea that the electrons, with a series of scattering events, cross the central region with a probability $T(E,V)$, by the means of transmission channels provided by available energy level in the central region that, due to the interaction with the electrodes continuum and the presence of an external bias, that shifts the Fermi level of the aforementioned electrodes, move and broaden, as long as they interact

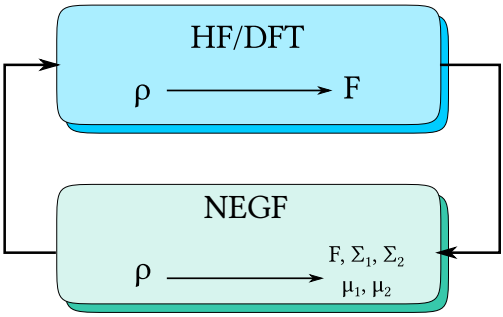

Figure 3.4: Self-consistent scheme used for electrode/channel/electrode calculations under external bias.[48]

with the leads. Energy levels that do not couple with lead states do not broaden into resonances, and are not "available" channels for the electrons to tunnel.

It is also important to remember that the whole method here described poses its foundation on a series of pretty strict approximations, which are not guaranteed to be satisfied for nanoscopic systems. In particular, all these approximations lead to a description of a system in which a steady state for the current is guaranteed to exist, condition which we don't know *a priori*. Also, they can only capture mean-field properties of electron dynamics, which is plausible in the case of non-interacting electrons, but not very accurate in case of interacting electrons.

The usual computational procedure involves a self-consistent scheme, implemented as follows:

1. Calculate the coupling terms V and the Surface Green's function for the electrode in order to obtain self-energies and Fermi levels, with a separate, periodic calculation on bulk material;

2. After calculating the self-energies for the electrodes, calculate eigenvalues and eigenvectors for the "extended" Hamiltonian

$\widehat{H}_{eff} = \widehat{H}_C - \widehat{\Sigma}_L(E) - \widehat{\Sigma}_R(E)$;

3. Using the eigenvalues and eigenvectors obtained at the previous step, calculate Green's function using:

$$\widehat{G}(\boldsymbol{r}, \boldsymbol{r'}, E) = \sum_n \frac{\Phi_n(\boldsymbol{r})\Phi_n^*(\boldsymbol{r})}{E - \varepsilon_n} \tag{3.51}$$

with Φ_n given by $\widehat{H}_{eff}\Phi_n = \varepsilon_n \Phi_n$

4. With the Green's Function, it is possible to find the electron density using:

$$D = -\frac{1}{\pi}\Im \int_{-\infty}^{+\infty} \left[\widehat{G}(E) f(E-\mu)\right] dE \tag{3.52}$$

5. Given the density matrix, it is possible to calculate the electric field $\varepsilon(\boldsymbol{r})$ across the junction by the means of the Poisson equation:

$$\boldsymbol{\nabla} \cdot (\varepsilon(\boldsymbol{r}) E(\boldsymbol{r})) = -4\pi\rho(\boldsymbol{r}) \tag{3.53}$$

with the Fermi levels (shifted by the external bias) as the boundary conditions for the differential equation;

6. Given the density matrix and the electric field across the junction, the starting Hamiltonian can be updated. The cycle starts again from Point 1, until convergence is reached;

7. When convergence is reached, with the Green's function and the self-energy operators, the broadening matrices $\Gamma_{L(R)}$ and the transmission function $T(E, V)$ are ready to be calculated. After that, the transmission functions needs to be integrated between the proper bias window in order to obtain the final current.

3.3 Implementation of the method: the FOXY code

The previous chapter has described the Landauer-Büttiker theory, and the usual computational route followed in many standard electron transport codes. The implementation of the Landauer theory requires a self-consistent scheme in which, after a full periodic calculation on both electrodes to obtain self-energies, the effective Hamiltonian, with the inclusion of the field term, is diagonalised at each step. The field is the result of a separate numerical solution of the Poisson equation in which the charge density is known and provided by a diagonalization of the Hamiltonian matrix obtained in the previous diagonalization step.

Since the Landauer-Büttiker theory is, essentially, a single-particle theory, it couples nicely with Density Functional Theory, which is a single-particle, mean-field and ground-state theory. But there is no clear answer to the question of how accurate is a ground state DFT calculation for our purposes, even if we make the assumption that all the approximation in the Landauer approach are satisfied (and can, in principle, provide an acceptable description of the dynamics of the true many-body system in an ideal steady-state), and even if we could have the exact ground state DFT functional for our case. This is because we are effectively using a ground state theory for a non-equilibrium problem (electron flow from reservoirs at different electrochemical potential).

There are many other subtle technical problems to which is best to keep an eye on. One of the main issues is the geometrical details of the contact. While in mesoscopic systems a difference of few atoms does not affect the total current in a significant way, in nanoscopic system even a single-atom change in the configuration of the junction can lead to very large differences in the current,[51] mainly due to partial electronic screening, that can cause large variations in the electrostatic potential at the contact region. This is why a good geometry optimization step is always required before

a transport calculation. And, even in the case of a good geometry optimization step available, there are not experimental informations which can help in determining the exact local geometry between the single molecule and the electrodes.

Moreover, there are problems related to the calculation of the electrostatic potential in the central region. Solving the Poisson equation requires boundary conditions: due to the partitioning of the system, as defined in the previous Section, the potential at the interface between electrodes and central region is the required condition. Since the Landauer approach assumes that the electrodes are, in fact, reservoirs, they have well defined electrochemical potentials, μ_L and μ_R, eventually shifted by an external bias. In order to use μ_L and μ_R as boundary conditions for the Poisson equation, many layers of electrode atoms are needed to be included in the calculation of the central region, so to move far away from the contact region, "screen" the effects introduced by the contact itself, and, in the outermost part of the central region (the one directly connected to the reservoirs), reach a "bulk-like" behaviour.

It is then clear that modified self-consistent DFT calculations on such complex structures (such as the one described in the previous Section), with hundreds of atoms, are cumbersome and time consuming, both for the calculation of the optimal geometry of the junction, and for the ground-state calculations. Most of the time, these type of calculations give also overestimated results,[52,53] due to the geometrical reasons explained above, and also due to the fundamental problems related to the use of DFT (namely, self-interaction problem[54–56] and excited state evaluation). Notice that a full calculation is needed for every different voltage applied to the system.

One may then focus on the response of the contacted molecule to an external bias rather than on the two metallic contacts and the complex molecule-lead interface and consider an approximate approach that simplifies the metal-molecule interaction. In this way it is possible to put the attention on the behaviour of the molecule itself and on the molecular reasons which lead to, for example, rectification and switching phenomena. The goal, then, is to set up a

low-cost computational approach which may be applied with confidence to a large variety of devices, simplifying the metal-molecule interaction while retaining all the essential physics of the charge transport due to the molecular bridge.

The approach here used is to combine Density Functional Theory calculations for the molecular system, with the Non-Equilibrium Green's Function Method (NEGF) and the Landauer-Büttiker formalism for quantum transport in nanostructures, in a simplified way, as implemented in the domestic FOXY code.[57] This simplified technique has been created with the idea of developing a computationally efficient method for the calculation of I/V characteristics, which can be applied to a wider variety of molecular systems. This may allow a rapid, but reliable, investigation of molecules of potential application in electronic devices for their functionality.

The choice of Density Functional Theory as the main tool to calculate electronic properties of the central region means that we are going to use an effective ground state, single-particle Hamiltonian for the system even if the problem is intrinsically a many-body one, and out of equilibrium. Also, it implies the choice of a suitable exchange-correlation functional (which, however, are usually tailored for ground-state calculations).

We have applied an approximate treatment of the molecule-lead interaction whereas the voltage bias has been accounted for through a constant electric field. Starting from the method by Gonzales *et al.*,[58] where the molecule-lead coupling is taken independent from the energy and proportional to the projection of the molecular orbitals onto the terminal fragments of the molecule in between, we have developed the method described below. This approach can also be seen as a simplified derivation of the one based on the frontier orbitals of Ref.[59] and by virtue of its simplicity, its range of application may be thought to cover quite large molecular species.

According to the Newns-Anderson model,[60,61] adopted in the paper of Gonzales *et al.*,[58] we consider the interaction of a number of discrete orbitals φ of the molecule under study with a continuum of states ϕ_ε (normalized: $\langle \phi_\varepsilon | \phi_\varepsilon^{'} \rangle = \delta(\varepsilon - \varepsilon^{'})$) of an electrode. We

make here the first assumption:

Approximation 1 *The field generated in our system from an external bias is determined assuming the electrodes as two infinite parallel plates with an applied potential difference V, and the distance between the plates is the distance between the electrodes. The field which our molecule feels is therefore uniform, perpendicular to the surface of the electrodes (longitudinal to the molecule), and directly added into the Kohn-Sham equations.*

We have then to solve the eigenvalue problem for both of the leads and the molecule:

$$\widehat{H} = \widehat{H}_C + \widehat{H}_L + \widehat{H}_R + \widehat{V}_{LC} + \widehat{V}_{CR} \tag{3.54}$$

$$\widehat{H}_C|\varphi_j\rangle = \varepsilon_j|\varphi_j\rangle \tag{3.55}$$

$$\widehat{H}_{L(R)}|\phi_{\varepsilon,L(R)}\rangle = \varepsilon|\phi_{\varepsilon,L(R)}\rangle \tag{3.56}$$

where $\widehat{H}_C$ and $\widehat{H}_{L(R)}$ are suitable one-electron Hamiltonians describing the molecule and the left (right) electrode (assumed to be identical) and the V terms represent the coupling between the leads and the central molecule (neglecting direct lead-lead coupling, as described in the previous section). In the framework of the so called "extended molecule" model, the central molecule may also include a small portion of the electrodes, in order to take into account at least part of the electronic rearrangement due to bonding between the molecule and the leads. Since the ϕs are the eigenstates of a one-electron Hamiltonian, the corresponding unperturbed Green's function is diagonal in the ϕ basis and the self-energy is (for the time being we consider only one electrode):

$$\Sigma_{L(R)} = V^{\dagger}_{LC(CR)} G_{L(R)} V_{LC(CR)} \tag{3.57}$$

here $V_{LC(CR)}$ are the coupling matrices and $G_{L(R)}$ is the Green's function for the electrodes. $G_{L(R)}$ can be written in an alternative

form with respect to the general one (see Eq.3.43):

$$G_{L(R)} = \sum_{\varepsilon} \frac{|\phi_{\varepsilon,L(R)}\rangle\langle\phi_{\varepsilon,L(R)}|}{E-\varepsilon+\imath\delta} = \int \frac{|\phi_{\varepsilon,L(R)}\rangle\langle\phi_{\varepsilon,L(R)}|}{E-\varepsilon+\imath\delta} d\varepsilon \quad (3.58)$$

where δ is a positive infinitesimal constant. The self-energy therefore is (dropping the $L(R)$ suffixes for simplicity, whenever possible):

$$\Sigma = \int \frac{V^{\dagger}|\phi_{\varepsilon}\rangle\langle\phi_{\varepsilon}|V}{E-\varepsilon+\imath\delta} d\varepsilon \quad (3.59)$$

which becomes, after projection onto the H_C eigenstates:

$$\Sigma_{jk}(E) = \int \frac{V_{j\varepsilon}V_{\varepsilon k}}{E+i\delta-\varepsilon} d\varepsilon \quad (3.60)$$

where $V_{j\varepsilon} = \langle\varphi_j|V|\phi_{\varepsilon}\rangle$. The integral can be recast as:

$$\Sigma_{jk}(E) = \int \frac{V_{j\varepsilon}V_{\varepsilon k}}{E+i\delta-\varepsilon} d\varepsilon = P\int \frac{V_{j\varepsilon}V_{\varepsilon k}}{E-\varepsilon} d\varepsilon + \imath\pi V_{jE}V_{Ek} \quad (3.61)$$

where P denotes the Cauchy principal value. Here we need to make another approximation:

Approximation 2 *The coupling terms $V_{j\varepsilon}$ are independent from the energy.*

Given that, the first term of Eq.3.61 vanishes, leaving only the imaginary part, and therefore making the self-energies independent from energy:

$$\Sigma_{jk} = \imath\pi V_j^* V_k \quad (3.62)$$

where V_j is the value of $V_{j\varepsilon}$. With the approximations employed, we have purely imaginary self-energies: this means that the levels are only broadened and not shifted.

Now, we introduce the approximation proposed by Gonzales *et al.*:[58]

Approximation 3 *V_j is assumed to be proportional to the projection of φ_js onto a a terminal fragment of the molecule close to the considered electrode.*

One can then rewrite the self-energy matrix as:

$$\Sigma_{jk} = -\imath\frac{\Delta}{2}\langle P\varphi_j|P\varphi_k\rangle = -\imath\frac{\Delta}{2}Q_{jk} \tag{3.63}$$

where P is the projection operator for the considered terminal fragment and Δ is an empirical constant that accounts for the molecule-lead interaction. The broadening matrix then becomes:

$$\Gamma_{jk}^{L(R)} = \Delta Q_{jk}^{L(R)} \tag{3.64}$$

If we insert Eq.3.63 in Eq.3.43, we can calculate the transmission function wit Eq.3.50. First, making the further assumption that the Green's function is diagonal, we can evaluate it without matrix inversion as:

$$G_{jj}(E) = \left[E - \varepsilon_j - \imath\frac{\Delta}{2}\left(Q_{jj}^R + Q_{jj}^L\right)\right]^{-1} \tag{3.65}$$

and then the transmission function can be computed as:

$$\begin{aligned} T(E) &= \Delta^2 \mathrm{Trace}\left[Q^L G Q^R G^\dagger\right] \\ &= \Delta^2 \sum_{jk} Q_{jk}^R Q_{kj}^L \frac{(E-\varepsilon_j)(E-\varepsilon_k) + \Gamma_j\Gamma_k}{\left[(E-\varepsilon_j)^2 + \Gamma_j^2\right]\left[(E-\varepsilon_k)^2 + \Gamma_k^2\right]} \end{aligned} \tag{3.66}$$

where:

$$\Gamma_j = \frac{1}{2}\left(\Gamma_{jj}^L + \Gamma_{jj}^R\right) = \frac{\Delta}{2}\left(Q_{jj}^L + Q_{jj}^R\right) \tag{3.67}$$

The transport properties of the molecules of interest can then be computed by choosing a suitable effective Hamiltonian for the contacted molecule, projecting the molecular orbitals (MOs) on the left (right) fragment in order to calculate $Q_{jk}^{L(R)}$ and then use them

to calculate the transmission spectrum according to Eq.3.66. The dependence on the external bias is obtained performing DFT calculations at each value of the corresponding electric field applied to the contacted molecule.

In order to take explicitly into account the molecule-lead adsorption, we should consider an "extended" molecule where the molecule under study is terminated with an end-group and then attached to a small cluster of atoms belonging to the leads. All the "extra" atoms are added directly to the central region, with no need for electrode calculations.

It is then clear that the central quantities of our model are the projections of the molecular orbitals onto the terminal fragments, from which the self-energies Σ (as well as the broadening Γ and the transmission function $T(E,V)$) strictly depend. The previously introduced Δ parameter only plays the role of an extended molecule-infinite lead coupling parameter, and, once set by a calibration procedure, it should be kept frozen for every system which employs electrodes of the same kind as the one used for the calibration, and the same terminal atom for the central molecule. For example, we can calibrate our method on experimental data for the well-known benzene di-thiol molecule coupled with Gold leads. Once the calibration for the Δ is over, the value found should be used for every species bonded with semi-infinite Gold electrodes. The issue of the calibration of the method is described in detail in the next Chapter.

In order to correctly project the molecular orbitals onto the terminal fragments, the atoms of the extended molecule are partitioned into three classes: left (L, atoms closest to the left electrode), right (R, atoms closest to the right electrode) and channel (C, atoms of the proper central region). The idea is to use a strategy based on Mulliken population analysis,[62] where the atomic orbital basis set is partitioned in functions centred on L, R or C atoms. The molecular

orbitals (MOs) can be written as:

$$|\varphi_j\rangle = |\chi^L \chi^C \chi^R\rangle \begin{bmatrix} C_{Lj} \\ C_{Cj} \\ C_{Rj} \end{bmatrix} \tag{3.68}$$

and the overlap between two MOs can be written as:

$$\langle\varphi_j|\varphi_k\rangle = C^*_{Lj} S_{LL} C_{Lk} + \frac{1}{2}\left(C^*_{Lj} S_{LC} C_{Ck} + C^*_{Cj} S_{CL} C_{Lk}\right) \tag{3.69}$$

$$+ C^*_{Cj} S_{CC} C_{Ck} + \frac{1}{2}\left(C^*_{Lj} S_{LC} C_{Ck} + C^*_{Cj} S_{CL} C_{Lk}\right) \tag{3.70}$$

$$+ \frac{1}{2}\left(C^*_{Rj} S_{RC} C_{Ck} + C^*_{Cj} S_{CR} C_{Rk}\right) \tag{3.71}$$

$$+ C^*_{Rj} S_{RR} C_{Rk} + \frac{1}{2}\left(C^*_{Rj} S_{RC} C_{Ck} + C^*_{Cj} S_{CR} C_{Rk}\right) \tag{3.72}$$

identifying the first row as the contribution to the overlap given by the L fragment, the second and the third one as the contribution by the C fragment and the fourth one as the contribution by the R fragment. In order to get, for example, the right projected matrix element, we only need to sum:

$$Q^R_{jk} = C^*_{Rj} S_{RR} C_{Rk} + \frac{1}{2}\left(C^*_{Rj} S_{RC} C_{Ck} + C^*_{Cj} S_{CR} C_{Rk}\right) \tag{3.73}$$

These elements also have the property:

$$Q^L_{jk} + Q^C_{jk} + Q^R_{jk} = \delta_{jk} \tag{3.74}$$

with δ_{jk} as the Mulliken atomic charges.

3.3.1 Implementation in the Gaussian package

With all the equations at hand, it is clear that the FOXY method speeds up the calculations of transport properties of molecules between metallic leads. The price we have to pay is in a minor accuracy in the calculations. The procedure here is to run DFT calculations

for each separate value of the bias in which we are interested, and calculate the corresponding transmission function and current. The I/V characteristic is then the result of several DFT calculations on the extended molecule, followed by a FOXY calculation. Considering that a full DFT-NEGF self-consistent procedure is computationally expensive (which, depending on the machine in which they are running, could be even days long for a single bias point), the entire process that we employ cuts down the computational time for the complete I/V characteristic significantly (even in the worst cases of big and long molecules), where most of the computational time is dedicated to solve the DFT problem. In fact, FOXY calculations, with respect to ground-state self-consistent DFT calculations, are much faster, even for molecules with more than a hundred atoms, thanks to dedicated routines for multiple matrix multiplications of the $A^{\dagger}BA$ type (multiple matrix multiplication is particularly needed in the $Q_{L(R)}$ calculation).

As he calculation of the current is performed by an numerical integration of Eq. 3.25 on a finite grid, some inaccuracies due to very small and narrow peaks can take place. The problem has been tackled with a new procedure, where the Γ_j terms of Eq.3.67 are not tested against a threshold value, but the whole transmission function is convoluted with a Gaussian with FWHM provided by the user. In order to properly employ the convolution operation, a selective refinement of the energy grid (set for the integration of the $T(E,V)$ over energy, as in Eq.3.26) was needed. The new grid scheme starts from the one generated by the main program, with a spacing between adjacent points provided by the user, and then superimposes it a new grid, refined around the peaks of the transmission function. This new operation is controlled by two new external keywords, which define the interval, in energy, around a peak of the $T(E,V)$ where the grid should be refined, and the number of new points to be added to the original energy grid.

Another parameter that is free and needs to be provided by the user is the value of the Fermi energy ε_F. Standard self-consistent codes employ separate calculations on leads in order to calculate

self-energies and Fermi levels, which are used as boundary conditions for calculations of the potential in the central region and to the calculation of the overall Fermi level of the entire structure. The fact that with the FOXY method calculation on the periodic leads are completely avoided, means that there is not a strict procedure to calculate Fermi levels of such leads, and consequently of the entire structure. Fermi energy is a critical point in electron transport calculations, because it defines the starting point for which the integration bias window is defined (see Eq.3.26): it could be misleading to take the Fermi level of the entire system as the Fermi level of the central molecule, because the energy of half the HOMO-LUMO gap does not take into account the interaction of the molecule with the (periodic, semi-infinite) electrodes. By the way, keeping the Fermi level as half the HOMO-LUMO gap of the extended molecule (molecule plus few atoms of the leads) can be a reasonable guess when experimental information on the systems under study are not available.[63,64] Since with FOXY code it is not possible to calculate the Fermi level of the metal/molecule/metal, a reasonable approximation for ε_F is to take Fermi levels derived from experiments or accurate calculations on bulk materials.[65] Since the Fermi level of the bulk electrodes material neither is the real Fermi level of the entire metal/molecule/metal system, and since it can lay out of the HOMO-LUMO gap, and since our method does not take into account charging effects for the central molecule (which can induce a change, other than the one caused by an external electric field, occupied and virtual levels positioning), small variations on the Fermi level can be applied in order to make it lay inside the molecular HOMO-LUMO gap. We think that the fact that the Fermi level can be outside the calculated HOMO-LUMO gap of the extended molecule can be caused by an insufficient level-shifting, due to the fact that, in our method, we consider only small Gold clusters instead of full semi-infinite electrodes. Of course, this procedure should be employed keeping in mind the fundamental problems of DFT, in particular regarding the positioning of virtual levels and the evaluation of the HOMO-LUMO gap: with these fundamental drawbacks, a complete

agreement, it is really hard a possibility, even if self-interaction corrected functionals[54–56] are employed in the calculations. Noticing that the transmission function is independent on the position of the Fermi level, and can be considered as the reference quantity in an absolute energy scale, we use, as Fermi level, the midpoint of the HOMO and LUMO orbital energies.

In our case, Au electrodes are employed, so the starting value of the Fermi level is -5.3 eV (value of the Fermi level of bulk gold, as taken from literature), with possible variations that depends on the nature of the molecular system (see Chapter 4 for more details). It should be kept in mind that the calculation of the transmission function $T(E, V)$ is not affected by the choice of the Fermi energy of the extended system. The position of the Fermi energy has even been considered as an adjustable parameter of the model.[66] Only the evaluation of the I/V curve depends directly by the Fermi level position. We can then consider $T(E, V)$ as the main reference quantity in our transport calculations. The effects due to these approximations for the evaluation of the Fermi level are expected to have a minimal impact on qualitative comparisons between different molecules, as long as the same set of approximations is used throughout.

It is clear that calibration procedures are necessary in order to define the proper Δ value to use, and to determine which FWHM and grid values provide the most stable results.

The entire code has been implemented also in a locally modified development version of the GAUSSIAN09 code,[67] with a complete rewriting of the main routine and the corresponding subroutines. The only data that the FOXY program (in its stand-alone version) needs are orbital energies (α and β, if an unrestricted calculation is chosen), orbital coefficients (α and β for unrestricted calculations), easily obtained from Hartree-Fock or DFT calculation. In the GAUSSIAN implementation, it internally interfaces with the standard internal GAUSSIAN array where these informations are stored during the execution of the various routines. The overlap matrix is also needed, in order to compute the projections onto the fragments (see Eq.3.69).

Chapter 4

Application of the method to molecules of interest

Results are like shooting stars: you need a sharp look to search for them, you have to be patient to wait them out, and you need a little bit of luck to admire their beauty.

Livia Vallini

One of the simplest electronic circuital element is the rectifier (or *diode*), a passive device in which electrical current is allowed to flow in only one direction. This is also the first type of device that has historically been attempted to be made with single molecules. In 1974, Aviram and Ratner[3] were the first to suggest an organic molecular system showing current rectification, composed by a "donor" and an "acceptor" group attached by a carbon bridge with single bonds. By

studying this organic analogue of a p-n semiconductor junction, they envisioned the charge transport as a three-step process, consisting of electron and hole injection into the acceptor and donor segments of the molecule, and easy electron transfer will be in the acceptor to donor direction, because of the lower oxidation potential of the donor segment (its molecular levels are higher in energy).

We may think at molecular rectification as the initial step of molecular electronics. Due to the difficulties of building efficient molecular rectifiers,[68] the research in the field is still very active.[69–75] In this perspective, we want to investigate, with our simplified approach, the rectification properties of molecular species.

In this chapter, we will present testing and calibration of the method presented in the previous chapter, done with calculations on the prototypical system for molecular transport calculations and experiments, benzene dithiol (BDT), which consists in a benzene ring with the Hydrogen in 1- and 4- position substituted with a -SH group. A cluster of three Gold atoms (Au-Au = 2.88 as in a typical (111)-Au surface[76]) was added at each end of the molecule (Fig. 4.1, top), with the Sulphur bonded in hollow position at each side of the bare molecule. In this way some effects of the electronic rearrangement due to the molecule-lead bonds are explicitly included in the theoretical calculation. The calibration has been done with direct comparison between the computed I/V characteristics and the one measured by Reed *et al.*,[77] in order to find the optimal value for the parameter Δ.

Once the optimal value was found, the molecular diode synthesized and probed by Weber *et al.*[5] has been studied.[78] Even for this molecule the -SAu_3 ending group was added to the relaxed structure of the isolated molecule. The experimental data reveal that this species is characterized by a small conductivity but a significant rectification ratio in the range of $\pm 1.5V$ of the applied bias voltage. Despite the simplicity of our approach, we have been able to reproduce the experimental results and to analyse the chemical reasons of the observed rectification.

We also started to study which species can be made asymmetric

by mixing different metals in the channel region, as well as substituent groups, in particular electron-acceptor groups (such as Fluorine). As a bridging ligand between these metals, we have chosen pyrazine, well know from the mixed-valence chemistry,[79] and as ancillary ligands we have considered porphirazine in order to have a neutral molecule with the metals in oxidation state II. The contact to the gold electrodes is obtained by two terminal thiol-pyridine ligands. Depending on the type of the metals used, the I/V curves show a symmetric or a asymmetric behaviour (with relevant bias-dependent rectification ratio significant only in a limited bias window). This feature can be explained considering the relative positioning of the relevant occupied energy levels of the metallic fragments, which interact in the formation of delocalized orbitals of the supermolecule that acts as conduction channels.

4.1 Calibration of the method

Due to the presence of the empirical parameter Δ, as introduced in Eq.3.63, the need of tuning grid values for the integration of the $T(E,V)$ and the evaluation of the Fermi level of the system, the practical implementation requires a preliminary calibration. For the calibration of the Δ parameter, this might be done in two ways:

- By comparing, for a benchmark molecule, the I/V curve computed at various values of the parameter, with experimental references (such as[77]);
- By comparing the aforementioned computed I/V curve with NEGF-DFT results obtained by programs that calculate metal-molecule self-energies including explicitly the metallic contact, and in fact employing the self-consistent scheme described in Chapter 3 (like, e.g. that available in the TranSIESTA code[80] or in the ATK package[81]).

Due to the known problems of DFT (such as self-interaction and image charges) which may affect the energy level positioning and there-

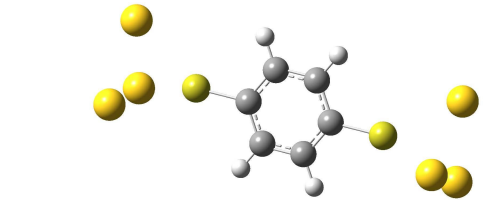

(a)

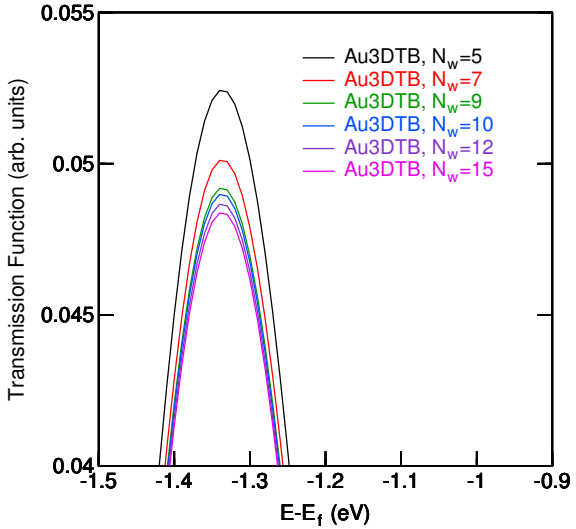

(b)

Figure 4.1: (a) Benzene Di-thiol molecule, with the cluster of Au atoms used for the calibrations, as explained in Section 4.1. (Au=yellow, C=grey, H=white, S=olive); (b) Detail of the Au_3DTB transmission function, varying the energy interval where the grid should be refined. Here, the N_p parameter (previously calibrated) has been taken fixed. Notice that, after a value of 12, further increase of this parameter doesn't affect the precision of the curve.

fore the computed I/V curve, we decided to calibrate our method with respect to experiments, being well aware that also experiments may have issues. In fact, we don't know yet the exact nature and the geometry of the metal-molecule interface.

For calibration we have selected benzene 1,4-dithiol (DTB) and modelled the metallic junctions by two clusters of three Gold atoms (as described above) at each end (Au_3DTB, from now on), and performed calculations at different values of Δ. The results have been compared with the experimental data by Reed *et al.*[77] which, according to the authors, are averaged on several different measurements and well reproducible.

All calculations, including geometry optimization at zero bias, have been performed using the B3LYP functional, LANL2DZ basis set[82] for Au and 6-311G* basis set for the remaining atoms. We have taken $\varepsilon_F = -5.3$ eV as the starting value of the Fermi level of the lead-molecule-lead system. In our work we define as positive a current flowing from the left lead to the right lead, so that a positive voltage lowers the Fermi level of the left contact and increases that of the right contact. All DFT calculations (geometry optimization and single-point calculations) described in this work have been performed with the development version of the GAUSSIAN suite of programs.[67]

The grid points for the integration of the $T(E)$ were chosen in the following way. For each peak of the $T(E)$ a fixed number of points N_p was included in a energy interval equal to its FWHM and this energy range was replicated for a number of FWHMs N_w around the energy of the peak. The grid points of all peaks were then merged in a unique grid after elimination of the points excessively closed to each other. Test were performed in order to reach convergence, that means a grid density such that a further increase of the density does not yield significant changes in the $T(E)$ (Fig. 4.1, bottom). The best values for the parameters are $N_p = 200$ and $N_w = 12$.

After the calibration of the grid parameters, we started to calculate the transmission function of the DTB molecule for various

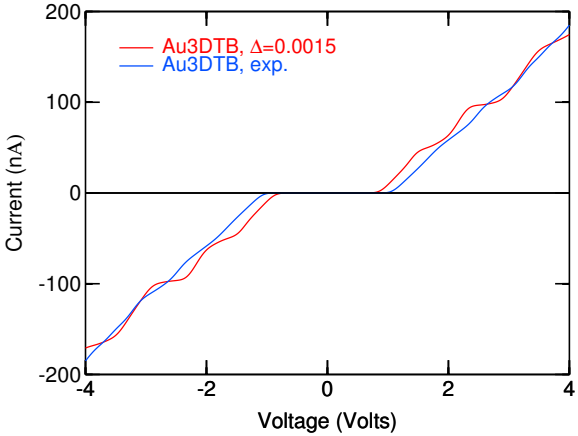

Figure 4.2: I/V characteristics of the Au3DTB molecule obtained with the FOXY code, with $\Delta = 0.0015$ (as the experimental I/V curves for the Au3DTB[77])

values of the Δ parameter, aiming at reproducing the experimental curves.[77] The obtained I/V characteristic is reported in Fig. 4.2, where the computed curve is in strong agreement with the experimental one, in particular for the initial energy gap (of about $2V$ near the Fermi level). The only difference is in the "smoothness" of the curve: this could be related to the precision of the working apparatus employed in the experimental probing of the molecule or either in the approximation we have made regarding the metallic contact and the molecule-lead coupling. The FOXY method, however, can highlight the current steps related to the broadened molecular levels that enter the bias window. The Δ parameter used is $\Delta = 0.0015$ and this value is therefore used also in the subsequent calculations (the curve with the coupling $\Delta = 0.75$ differs quantitatively, and has not a net gap around ϵ_f).

4.2 Molecular Rectifiers

With the aim of investigating the rectification mechanism in molecules, we studied the molecular rectifier synthesized and probed by Weber *et al.*[5,78] Even in this case, all calculations, including geometry optimization at zero bias, have been performed using the B3LYP functional, LANL2DZ basis set[82] for Au and 6-311G* basis set for the remaining atoms.

As explained before, in order to calculate the I(V) curve, it is important to know the positioning of the Fermi level with respect to the molecular orbitals of the system under study. Although one may reasonably expect that the Fermi level in a molecular junction lies somewhere in between the HOMO and LUMO energies[66] so to minimize charging effects, the determination of its exact position is not straightforward. This is especially true when the bulk Gold is represented with a small cluster of few atoms as presented here. However, in many cases the experimental value of the Gold Fermi energy is found in between the HOMO and LUMO energies of the extended molecule (molecule plus Gold clusters). Usually, when possible (so, when it lies into the HOMO-LUMO gap), in FOXY calculation we try to pin the value of the Fermi level of the system to the one of the bulk Gold ($\sim$-5.3 eV), but it is usually used also ad a fitting parameter hen experimental data are accessible. In this case, we find out that a value of -5 eV is right to correctly reproduce the experimental I/V curves.

The optimized structure of the molecule (Fig. 4.3) shows that the two central rings are nearly orthogonal due to the steric hindrance of the ortho methyl groups. In this conformation, the left and right parts of the molecule have almost independent π orbital systems and, as expected, only a negligible current is found (it is well known that, in order to obtain small but not negligible current flow across a molecule, delocalized orbitals capable of couple to both ends of the junction are needed, so that the electrons can easily flow from an electrode to the other). This is, however, different from the

significant currents observed in the experiments. We may then suppose that in the experimental setup the molecule is displaced from the optimized angle. In order to find the actual value of the central torsional angle, we repeated the calculations for different angle values, with steps of 15 degrees each, and then computing the I/V characteristics. We found that at 105 we can obtain currents in the range of the experimental values (Fig. 4.3).

Although the distorted structure is less stable than the minimum energy one by 0.022 eV ($\approx$ 0.5 Kcal/mol), and it is thus not sufficiently populated at the temperature (30 K) of the experiment,[5] it is evident from the physics of the system that the two central rings must be displaced from the optimized perpendicular conformation in order to get detectable current flow across the molecule.

From Fig. 4.3 it is apparent that the I/V curve for the 105-species is highly asymmetric, revealing a diode-like behaviour (rectification), where the carrier flow is inhibited for positive voltages. For negative voltages, the computed current, after an initial gap, shows a net increase at $\approx -0.8V$, with a rapid grow for more negative biases (up to -7 nA). The calculated rectification ratio, defined as $I(-2V)/I(+2V)$, is $\approx$ 6.5, in good agreement with the value of 4.5 reported in[5] and referred to at $1.5V$ bias.

The rectifying behaviour can be explained by looking at the transmission function $T(E, V)$ for $+2V$, $0V$ and $-2V$ reported in Fig. 4.4.[78] According to Eq.3.66 , $T(E)$ provides significant contributions in the integration energy range of Eq.3.26, when the product of the Q_L and Q_R matrix elements is significant in that region. This occurs for MOs delocalized in both the two Au_3 fragments, provided that destructive interference between MOs does not occur (see also Tab.**??** for details about orbital projections onto the terminal fragments). In Figs. 4.5, 4.5, 4.7 the orbitals and ϵ_f are shown for three values of the bias: +2V, 0V and -2V).

For each voltage, the HOMO and LUMO are the only orbitals inside the voltage window ($1V$) that slightly couple with both fragments, and their shape changes with the external bias. Increasing the bias, new orbitals come into play and start to couple with

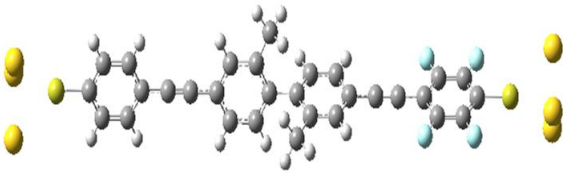

(a) Weber Diode

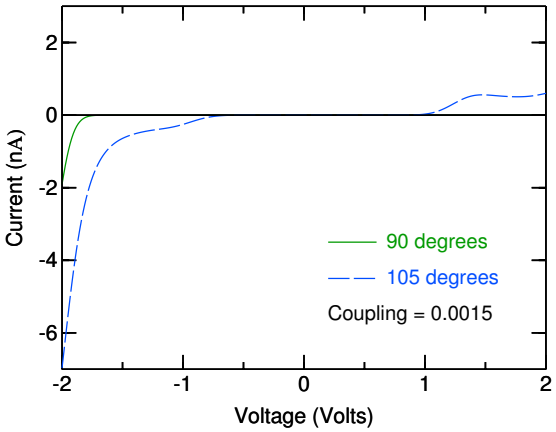

(b) I/V curves

Figure 4.3: (a) Molecular diode of.[5] In the figure we also show the three Au atoms placed on both sides of the molecule. The S atom is in hollow position with respect to the three Au atoms (Au=yellow, C=grey, H=white, S=olive, F=light blue); (b) I/V curves of the molecule under study for a torsional angle of 90 (continuous line) and 105 (dashed line).

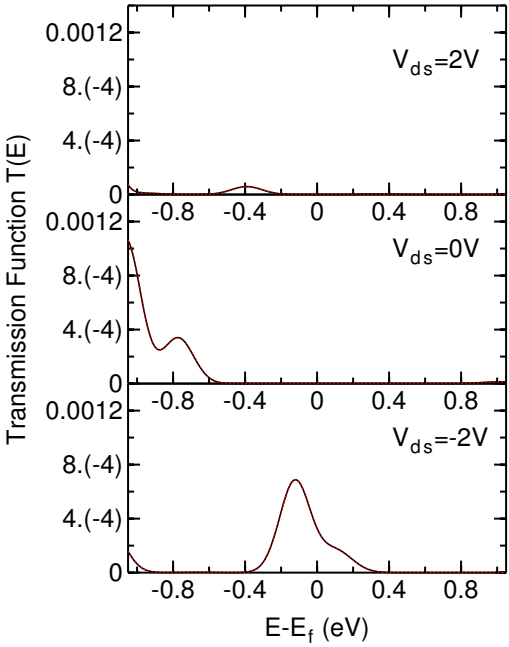

Figure 4.4: Transmission functions for the molecular diode with a torsional angle of 105, where it is clearly shown the asymmetry in the $T(E)$ for positive and negative biases (V_{ds}).

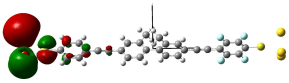

(a) LUMO+3

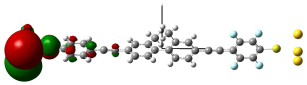

(b) LUMO+2

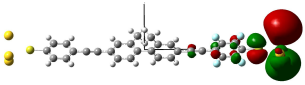

(c) LUMO+1

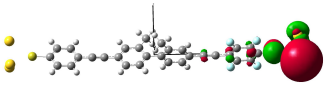

(d) LUMO

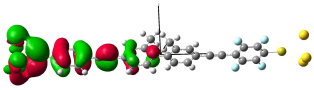

(e) HOMO

Figure 4.5: Weber diode orbitals at $-2V$ (Au=yellow, C=grey, H=white, S=olive, F=light blue).

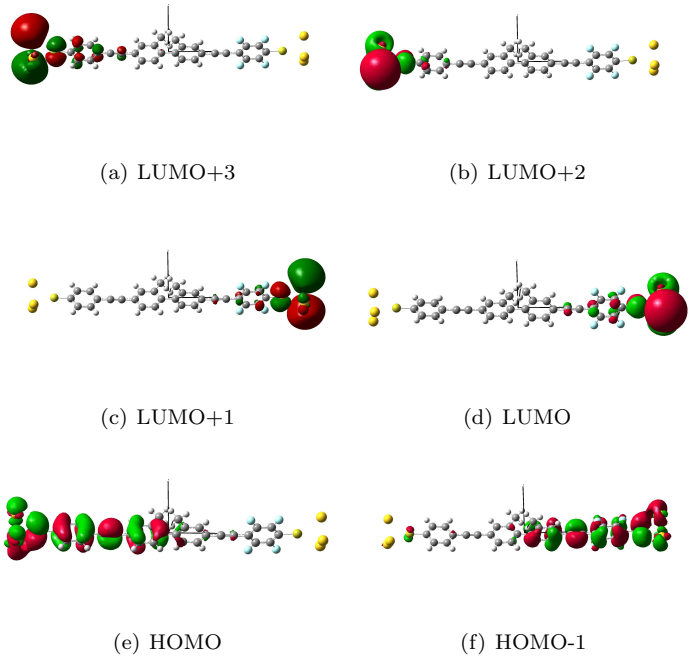

(a) LUMO+3 (b) LUMO+2

(c) LUMO+1 (d) LUMO

(e) HOMO (f) HOMO-1

Figure 4.6: Weber diode orbitals at $0V$ (Au=yellow, C=grey, H=white, S=olive, F=light blue).

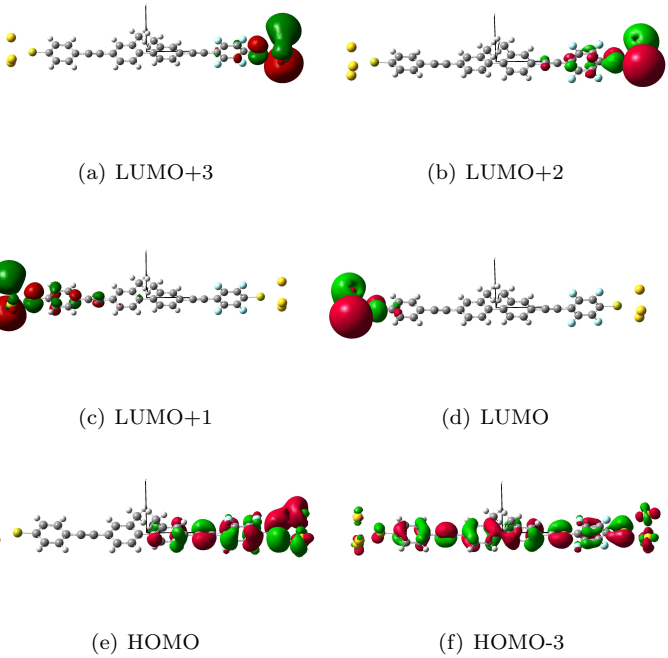

(a) LUMO+3 (b) LUMO+2

(c) LUMO+1 (d) LUMO

(e) HOMO (f) HOMO-3

Figure 4.7: Weber diode orbitals at $2V$ (Au=yellow, C=grey, H=white, S=olive, F=light blue).

the fragment atoms. At $0V$, the LUMO is localized on the right Au atoms (those closer to the fluorine atoms), whereas the HOMO is localized in the left part. For negative biases (up to $-2V$) the HOMO-LUMO gap decreases, the two orbitals undergo moderate polarization and the product $Q_L Q_R$, for both HOMO and LUMO, is small but sufficient (0.002 for the HOMO and 0.0012 for the LUMO) to give rise to a measurable current. $T(E)$ shows then a peak around ε_F (Fig.4.4). Other levels enter into the $\varepsilon_F \pm \frac{V}{2}$ window, but they do not couple with the leads, because they are mainly molecular or purely lead states, and so they are localized only in one part of the system.

The exact opposite behaviour is observed for positive biases. The HOMO-LUMO gap also decreases with respect to $0V$: the reason here is that HOMO and LUMO levels at $0V$ tend to be pushed far away from the Fermi energy by the field generated from negative biases, but virtual energy levels higher in energy at $0V$ than the LUMO are lowered by the field, and occupied levels that were lower in energy at $0V$ than the HOMO do the exact opposite. So, new levels become the HOMO and LUMO at $2V$ and the gap, effectively, decreases (Fig.4.7).

Also, for $2V$, the orbital polarization is the opposite, with the HOMO to the right and the LUMO to the left: the HOMO-1 at $0V$ rises up and becomes the HOMO, while the LUMO+3 at $0V$ lowers down and becomes the new LUMO. At the same time, the $Q_L Q_R$ product becomes very small in the range considered, because almost all the orbitals in the bias window do not couple with the leads (see Fig.4.7): this can also be seen from $T(E)$, where there is only a small peak ($\approx -0.4eV$).

The rectifying behaviour can thus be ascribed to the combined effect of the energy position of the relevant orbitals (HOMO and LUMO) and of their spatial extent, which determines the molecule-Gold coupling. In particular, the alignment of the HOMO and LUMO at $-2V$, which favours their mixing, seems to be the main element responsible for the computed rectification.

In order to deeply understand the rectification mechanism

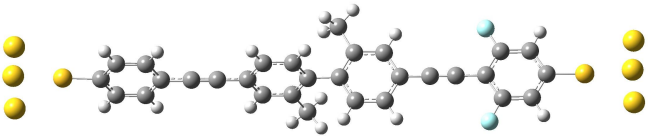

(a) A-species

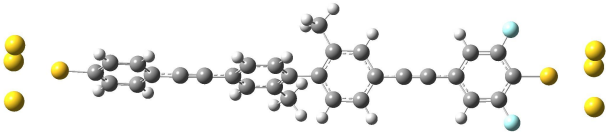

(b) B-species

Figure 4.8: Modified molecular species analyzed in order to better understand the role of the fluorine atoms (Au=yellow, C=grey, H=white, S=olive, F=light blue). (a) two fluorine atoms at the left of the rightmost benzene ring (A-species for now on), (b) two fluorine atoms at the right of the rightmost benzene ring (B-species for now on).

Orbital	Energy (eV)	Q_L	Q_R	$Q_L * Q_R$
		-2 Volts		
LUMO+1	-4.8402	0.0005	0.8000	0.0004
LUMO	-4.9135	0.0014	0.8200	0.0012
HOMO	-5.1223	0.2603	0.0076	0.0020
HOMO-1	-5.6601	0.7628	0.0000	0.0000
HOMO-2	-5.7617	0.4537	0.0000	0.0000
		0 Volt		
LUMO+2	-3.0889	0.0000	0.8176	0.0000
LUMO+1	-4.6488	0.7501	0.0000	0.0000
LUMO	-4.7373	0.8423	0.0000	0.0000
HOMO	-5.3908	0.0006	0.2394	0.0002
HOMO-1	5.9478	0.0001	0.6533	0.0000
HOMO-2	-5.9680	0.0000	0.5820	0.0000
HOMO-3	-6.2898	0.0547	0.1051	0.0057
		2 Volts		
LUMO+2	-3.7934	0.8368	0.0000	0.0000
LUMO	4.0280	0.0001	0.8209	0.0001
HOMO	-5.7716	0.2008	0.0036	0.0007
HOMO-1	-6.0653	0.0127	0.1689	0.0021

Table 4.1: Orbitals into the maximum integration window, with their projection onto the left and right fragments.

for this molecule, we investigated the effect of fluorine atoms more deeply, modifying the structure of the molecule: that is, removing two fluorine atoms at a time and repeating the set of calculations as above. The structures considered are shown in Fig.4.8, where the central torsional angle has been again fixed at 105, for reasoning explained before.

The I/V characteristics of the two species are reported in Fig. 4.9, where it is clear that the main transport features of the original molecule with 4 Fluorine atoms are reproduced in the system

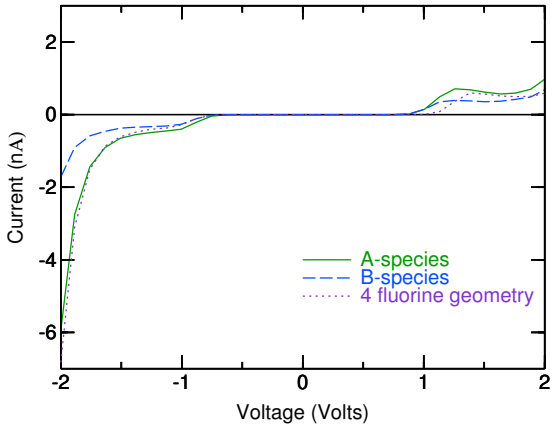

Figure 4.9: Current/Voltage characteristics for the A-molecule (continuous line) and B-molecule (dashed line). The I/V characteristic of the original molecule is also reported (dotted line).

with only two Fluorines placed in ortho positions with respect to the Sulphur atom, i.e. in the molecule A. This feature may find a qualitative explanation looking at the Mulliken charge distribution onto the substituted benzene ring. The Fluorine atoms (electron acceptors) in ortho positions determine an additional negative charge on the Carbon atom of the phenyl ring directly bonded to the acetylene linker and thus has driven electronic charge from the left part of the molecule towards the terminal ring coupled with the right lead (in Tab. **??**, Q_L of the HOMO is seen to double on going from 0 to $-2V$). This excess charge is easily transmitted through the remaining part of the molecule with a field capable of driving electrons from the left to the right electrode, without the need to pass through the central part of the molecule (where the π delocalization is broken). On the other hand, when the two Fluorine atoms are in meta positions as in the B structure, this effect is missing, no additional charge is ready to be easily transmitted, and the I/V curve is much

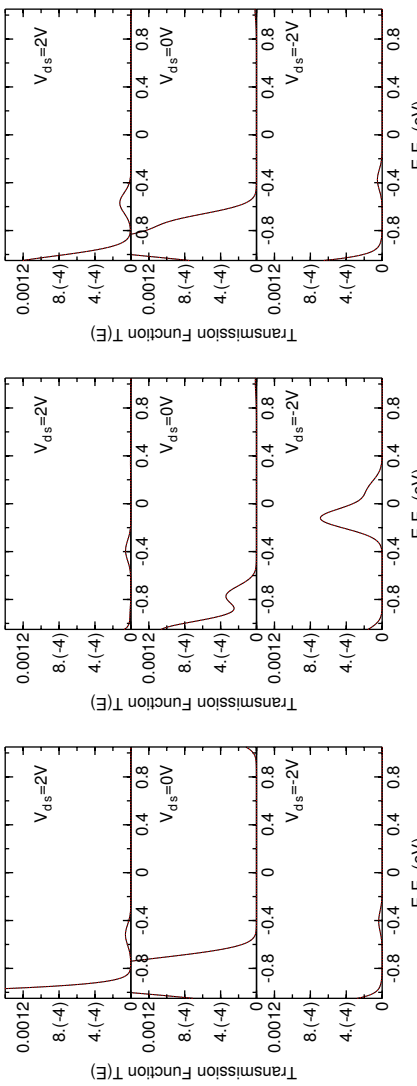

Figure 4.10: Comparisons between transmission function for the modified species and the starting one. Left: A-species, Center: original molecule, Right: B-species.

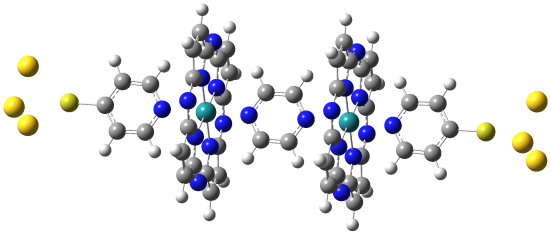

Figure 4.11: The Ru-Ru molecular system. The Ruthenium atoms are highlighted in turquoise blue. The other atoms are: N (blue), C (gray), H (white), S (olive), Au (yellow). All the other species are obtained substituting the Ru atom on the right with Os (Ru-Os) and with Fe (Ru-Fe). The field is applied along the z axis which contains both Sulphur atoms (left Sulphur at negative z, right Sulphur at positive z).

more symmetric.[78]

4.3 Binuclear transition metal complexes

Metal-ligand-metal species have been widely studied in the past, especially for their electrical and intramolecular electron and energy transfer processes.[83–87] What lacks is information about their conduction properties when properly contacted between metal electrodes, and their I/V characteristics and transmission properties.

We then decided to use the FOXY code to compute the transmission function and the I/V characteristics of molecular systems

of the kind outlined above, made by two binuclear transition metal complexes of the VIII group bridged by an aromatic ligand.[88] As a bridging ligand we have chosen pyrazine, and we have considered porphyrazine as ancillary ligands, in order to have a neutral molecule with the metals in the oxidation state II. The contact to the Gold electrodes is obtained by two terminal thiol-pyridine ligands, as shown in Fig. 4.11.

As far as we know, the systems discussed here have not yet been investigated experimentally. The reasons for the choice of this particular class of molecules is that, mixing different metals of the same group, we can assemble neutral symmetric and asymmetric systems and thus study the effects on the charge transport of the pure molecular asymmetry, without the complication of different electronic configuration in the valence shell. Such asymmetry may even be enhanced exploiting the use of terminal ligands with electron withdrawing substituents, as for instance in Ref.[78]

The three pairs of metals considered here are Ru-Ru, Ru-Os and Ru-Fe (see Fig. 4.11), which allow a comparison of the symmetric system (Ru-Ru) with the two non-symmetric species involving atoms of the same group, above and below Ru. Notice that along the whole paper, we will refer to the different species using for simplicity only the corresponding couple of metals in the order they appear in the molecule (e.g. Ru-Os means Ru on the left and Os on the right).

All DFT calculations (both geometry optimization and single point calculations) described in this work have been performed with the GAUSSIAN package,[67] whereas the transport properties have been obtained by our own FOXY code. The geometries of the systems have been optimized using the hybrid B3LYP functional, LANL2DZ basis set for Os, Ru, Au and Fe and 6-311*G basis set for the remaining atoms. The calculations at the several values of the bias were carried out at the same level of theory.

As stated in previous chapters, the choice of the Fermi level is critical, and, when experimental data are available, it can be treated s a "fitting parameter" in order to reproduce I/V curves. Unfortunately, the species here analysed don't have an experimental coun-

terpart. In absence of any possible comparison with experimental data and having to make a choice, we opted to place the Fermi level exactly in the middle of the HOMO-LUMO gap of the extended molecule, keeping it fixed for each value of the voltage. Nevertheless, the choice of the Fermi levels only affects the computation of the I/V curve without changing the transmission function, which can be considered as our reference quantities with respect to an absolute energy scale.

The standard trend in integrated circuits design tends to lower the reference voltage throughout the circuit, mainly for power consumption reasons. To date, 1.5V as reference voltage is quite common. We have then computed transmission spectra and current/voltage characteristics only up to 2V, as already done in a previous article.[78]

Fig. 4.12 (upper left) illustrates the I/V characteristics for the Ru-Os, Ru-Fe and Ru-Ru species. As expected (due to the fact that the Ru-Ru species is a symmetric molecule with respect to the z axis), the Ru-Ru molecule (blue line) shows a current symmetric with the sign of the bias. The Ru-Os and Ru-Fe molecules (green line and red line, respectively) are characterized by a non-symmetric I/V curves. For negative bias the current begin to flow at about the same value of V (which can be considered as a negative threshold voltage), whereas for positive biases the threshold of the onset of the current is different for the three species and goes opposite to the position of the right metal in the VIII group of the periodic table. This may find an explanation in the ionization potential of the different metals as discussed below, which reflects in the energy of the highest occupied orbital. In particular the HOMO corresponds to the highest orbital on the right metal centre for positive biases and to the highest orbital of the left metal centre for negative biases. As the left metal is always Ru, it may be expected that the effect of the different metals (right metal) on the current onset only occurs at positive biases. A direct consequence of this evidence is that the rectification ratio depends on the voltage, as shown in the upper right part of Fig. 4.12. In particular, whereas at the largest bias

considered, the effect of the different transition metals on the I/V characteristics is rather small (∼1.2 for the best case, Ru-Os), at smaller values of the voltage applied (around 1 Volt) we may notice a larger effect (right part of Fig. 4.12) due the different onset. Rectification of the same order but with larger currents has also been recently reported in the literature for different metallic-based systems.[89]

In the case of Ru-Os higher currents are observed for positive voltages, whereas in the case of Ru-Fe an opposite behaviour occurs. For Ru-Os, the comparison with the symmetric Ru-Ru species shows a net increase of the current for positive voltages and a less marked one for negative voltages, whereas for Ru-Fe system the opposite behaviour occurs.[88]

The I/V curves can be interpreted in terms of the corresponding transmission functions $T(E.V)$, reported in the lower part of Fig.4.12 for the three cases of Ru-Ru, Ru-Os and Ru-Fe, at the selected values of the external bias of -2V, 0V and 2V, respectively. In each figure the position of the Fermi level, as detailed in the previous section, is taken at halfway between the HOMO and LUMO energies and is indicated by a red vertical line, while the integration interval needed for the calculation of the current is delimited by the blue dashed lines.

The conduction properties of these systems in the investigated voltage range are determined by few molecular orbitals near the Fermi energy. At small biases, there is no peak in the integration range and thus a plateau with 0 current is observed in Fig.4.12. It is worthwhile noticing that for $V = 0$ the LUMO and LUMO+1 give rise to very large resonance peaks for each of the species (see Fig.4.12) that are completely destroyed by an even small bias and therefore do not contribute to the current. This phenomenon is mainly due to some interference (previously discussed in the appendix of Ref.[57]) and can occur for quasi-degenerate orbitals, whose mixing is given almost by accidental degeneration rather than by a true interaction between the terminal fragments.

As the voltage increases above a given threshold, the shape of the

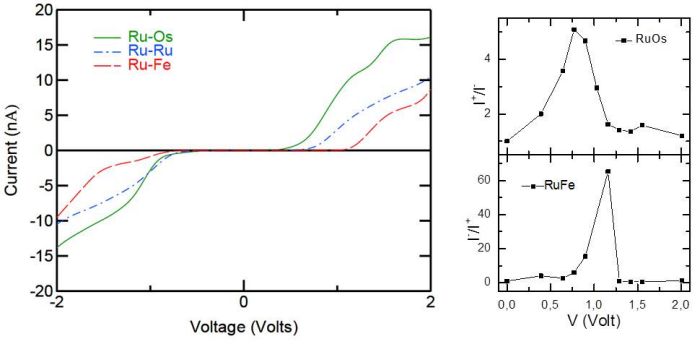

(a) I/V curves

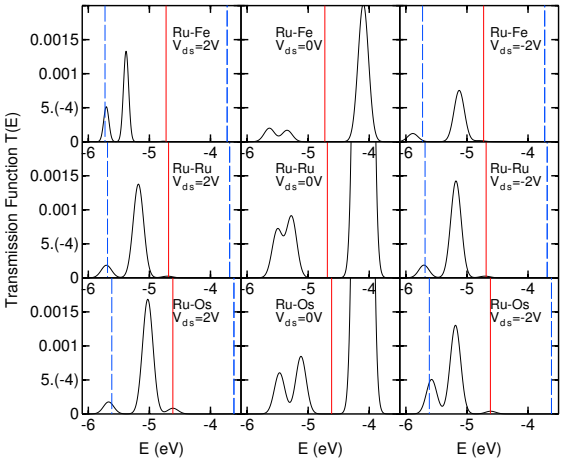

(b) $T(E, V)$ curves

Figure 4.12: (a) Left: current/voltage characteristics of Ru-Os (green continuous line), Ru-Fe (red dashed line) and Ru-Ru (blue dash dotted line) molecules. Right: rectification ratio for the two asymmetric species RuOs and RuFe (I^+:current for positive bias, I^-:current for negative bias). (b) Transmission functions of Ru-Fe (upper row), Ru-Os (lower row) and Ru-Ru (middle row) at +2V, 0V and -2V. The vertical red line show the position of the Fermi energy while the blue dashed lines indicate the limits of integration of Eq. 3.26.

transmission function changes and broadened resonant peaks enter the $[\epsilon_f - V/2, \epsilon_f + V/2]$ bias window at energies below the ϵ_f value. The transport mechanism may be interpreted as that of a transport mediated by holes (p-type) rather than electrons, since it involves only occupied orbitals. For the Ru-Ru system it is evident that the transmission function is irrespective of the sign of the bias. On the other hand, the $T(E)$ profiles of the Ru-Os and Ru-Fe species, are not much affected by the sign of the voltage and are consistent with the different values of the current and the small rectification observed in the I/V characteristics at $V = 2$ Volt. The band of the transmission function around ϵ_f at $V = -2V$ and $V = 2V$ is larger for Ru-Os than for Ru-Ru, and the contrary is seen for the Ru-Fe species, according to the overall larger currents for the Ru-Os and smaller currents for the Ru-Fe system, observed with respect to the symmetric Ru-Ru compound. As far as the rectification effect is concerned, we may notice in Fig. 4.12 that for the Ru-Os species the band at positive bias is slightly larger than that for negative V, while the opposite occurs for the Ru-Fe system. Therefore, it appears that the current is favoured in the direction that goes from the metal with lowest to that with highest atomic number (the reverse holds for the electron flow). This means that the rectification observed goes as in $D - \sigma - A$[90] and $\pi - \pi$ stacked[91] systems, but opposite to the Aviram-Ratner model.[3]

In Fig. 4.13 we may see, for the symmetric Ru-Ru system at $V = 0V$, few molecular orbitals around the Fermi energy Occupied MOs near ϵ_f (HOMO and HOMO-1 in Fig. 4) are basically of metallic-complex character while the empty MOs are essentially made by Au orbitals. The *p*-type conductivity in the bias range considered, related to the small component of Gold character of the MOs, is shown to involve the HOMO and the HOMO-1. In the lower part of Fig. 4.13, the energy of the orbitals localized on the two central metallic fragments[92] are reported to show how the rectification indeed goes opposite to the Aviram-Ratner scheme. We note that the HOMO energy for the three systems is driven by the metal with the lowest ionization potential (IP) and it is thus seen to increase in

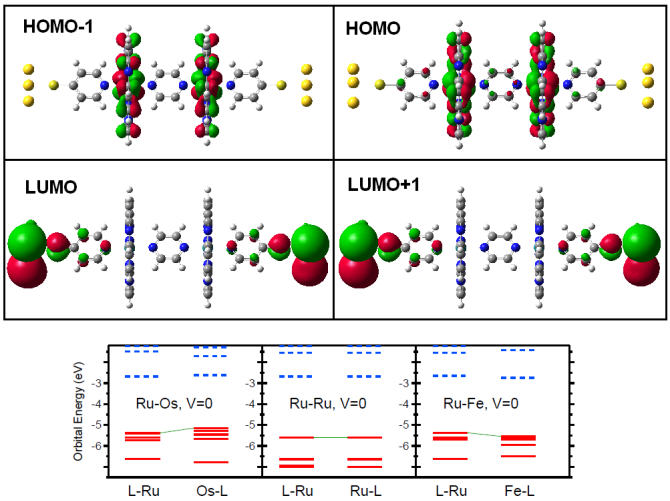

Figure 4.13: Top: MOs around the Fermi energy for the Ru-Ru system. Bottom: Energy level positions of the two metallic complexes for the three systems Ru-Os, Ru-Ru and Ru-Fe.

the order Ru-Fe < Ru-Ru < Ru-Os. The electron flow results then to be favoured in going from the metal with the lower IP (higher HOMO energy) to that with the higher IP (lower HOMO energy) while the opposite should be expected.

Looking at the previous results, it is clear that the asymmetric molecules studied here present only a small and well-defined region of the bias voltage around 1 Volt in which significant rectification can be achieved. Outside this region, rectification ratios fail to reach even the value of 2 (keeping in mind the limitation on the value of the rectification ratio obtained for molecules between metal leads discussed in the literature[?,93–96]). This means that, in order to exploit the capabilities of this class currents involved are very small,

of the order of nA, thus affecting practical applications.

With the aim to achieve a more stable behaviour, characterized by significant rectification in a broader range of voltages, one possibility is to introduce a suitable substituent groups at the ring of the fragments bridging the molecule to the leads.

Electron withdrawing or donor substituent have already been show to enhance the intramolecular donor/acceptor capabilities of bound molecular fragments and correspondingly the I/V asymmetry of the whole species.[5,78,90] We have then decided to investigate the I/V characteristics of possible analogues of the Ru-Ru, Ru-Fe and Ru-Os species in which four Fluorine atoms, are substituted to the corresponding Hydrogen atoms to the left or to the right outermost pyridine ring. Fluorine is not expected to induce significant perturbations on the molecular geometry, although its strong electronegativity could induce a relevant asymmetry in the molecule and enhance the rectification effect .

Fluorine substitution is made in the Ru-Ru, Ru-Os and Ru-Fe species, in order to probe the effect in a symmetric species but also in species that show small rectification per se. These new molecules, which will be named Ru-RuF Ru-OsF, FRu-Os, FRu-Fe, Ru-FeF in the text, depending on the transition metals used and the position of the F atom, are sketched in Fig. 4.14.

According to our previous considerations,[78] we expect that the effect of Fluorine is that of decreasing the electron flow from the side where Fluorine atoms have been placed and increasing it in the region where they are not present (the opposite holds for the current). For instance substitution on the RuRuF should favour negative currents. This effect was observed experimentally in a different fluorinated compound[5] and finds an explanation in the effect of the electron withdrawing substituent at the ring in favouring electron delocalization.[78]

The I/V characteristics of the RuRuF substituted species with its voltage-dependent rectification ratio, is reported in Fig. 4.15, where the results for the unsubstituted system are also reported, for comparison purposes. We can see that the behaviour of the sub-

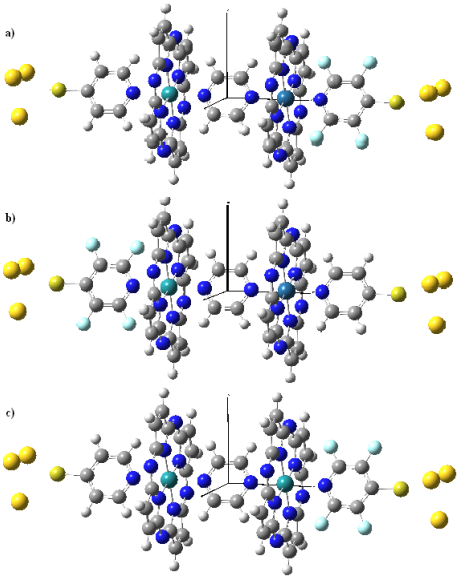

Figure 4.14: substituted species. a) Ru-OsF (F atoms to the right); b) FRu-Os (F atoms to the left); c) Ru-RuF. For the Ru-FeF and FRu-Fe species, the structure is the same, with Fe replacing Os (Au=yellow, C=grey, H=white, N=dark blue, S=olive, F=light blue, Ru=turquoise blue, Os=dark turquoise blue, Fe=violet).

stituted species is the one expected, with a clear reduction of the current in the direction of Fluorine, e.g. for positive bias where it also reaches a constant value, and an increase in the opposite case (e.g. for negative bias). This is accompanied by a reduction of the positive and negative threshold voltages for the onset of the current with respect to the unsubstituted case.

The rectification ratio reported in the upper right part of Fig. 4.15 shows a sudden increase for small currents at low bias, then a decrease and a further increase, with a maximum value of $\sim$4 at 2 V.

The consistency between the transmission function and the rectification ratios can be appreciated by looking at Fig. 4.15, where $T(E)$ is shown at 0 and 2 V for the Ru-RuF species and, for comparison also for the unsubstituted Ru-Ru system. The levels responsible for the conduction are the same in all cases, while the difference is in the heights of their corresponding peaks. At V=0 the two bands corresponding to the HOMO and HOMO-1 exchange their intensity in the species with Fluorine. However, it is more interesting to analyse the differences in the transmission function when in presence of the bias voltage. It is clear from the figure how at 2 V the $T(E)$ bands are much smaller for Ru-RuF then for Ru-Ru, while the opposite occurs at -2 V.

The effect of the Fluorine substitution in the Ru-Os and Ru-Fe systems is summarized in Fig 4.16, where the I/V characteristic curves and rectification ratios are reported for the various combinations.

As already observed for the Ru-Ru case, at small values of the bias where the electron flow begins, we can see a sudden increase in the rectification ratio followed by a decrease, with the only exception of the Ru-FeF species. For these values of the voltage the current is always very small (on the order of the nA) and the observed behaviour is due to the different rise of the current in proximity of the threshold voltage for conduction. As for the Ru-Ru system and according to our previous findings,[78] the effects of Fluorine substitution is that of decreasing the incoming current and increasing the

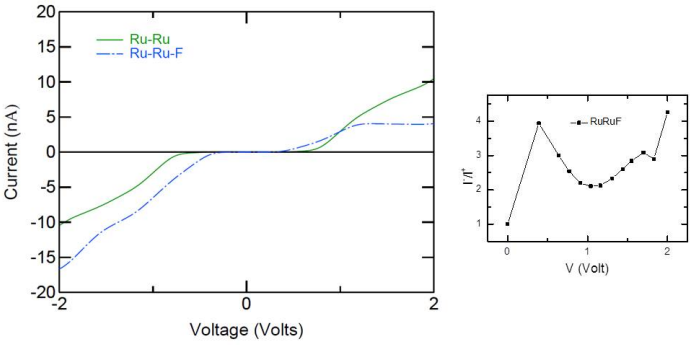

(a) I/V curve

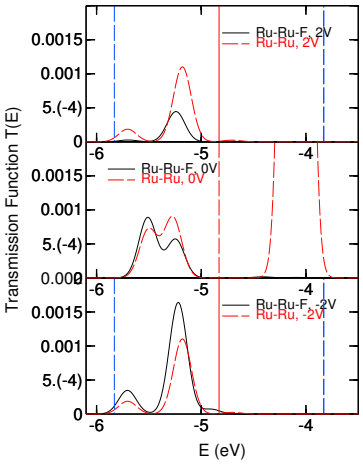

(b) $T(E, V)$

Figure 4.15: (a) Current/voltage characteristics of substituted Ru-Ru with F atoms on the right pyridine ring (blue dash dotted line). The curve for the unsubstituted species is also reported (green continuous line). (b) Transmission function for the Fluorine substitute Ru-Ru system (Ru-RuF. The values for the unsubstituded species are also reported for comparison (red dashed lines). The vertical red line show the position of the Fermi energy while the blue dashed lines indicate the limits of integration.

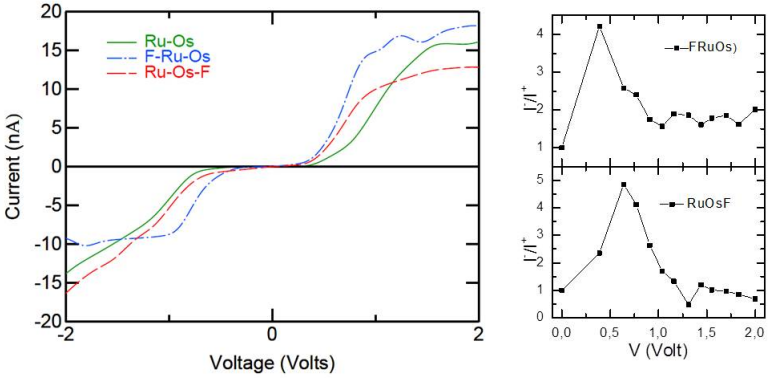

(a) TSC

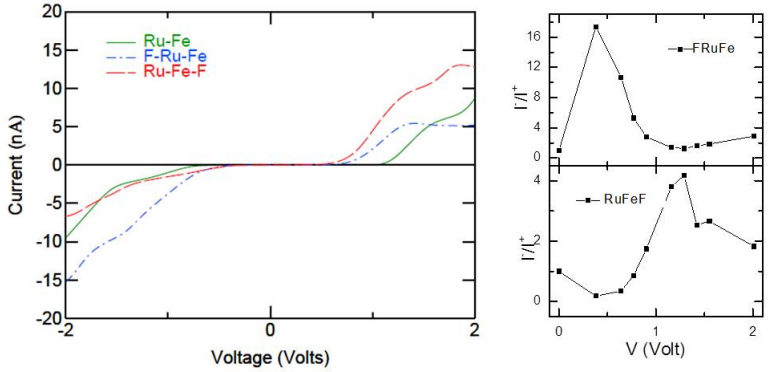

(b) 4Py

Figure 4.16: Current/voltage characteristics of substituted Ru-Os (top) and Ru-Fe (bottom) with F atoms on the left pyridine ring (blue dash-dotted line) or on the right pyridine ring (red dashed line). The curve for the unsubstituted species is also reported (green continuous line).

outgoing one.

The rectification ratio results to be significant only in a small range of voltage values, just as for the case without substitution reported in of Fig. **??**. The effect of Fluorine seems then only that of stabilizing the rectification for biases above 1 Volt at a value of about 2, only slightly higher than the value observed without substitution.

From the comparison of Figs. Fig. 4.15 and 4.16, we may conclude that the Ru-RuF species is that with the largest rectification at highest value of the bias, while more stable, although smaller, values are obtained for the non-symmetric species. In all cases we are however still far from values that would make these systems appealing for real application.

In synthesis, the symmetric species (Ru-Ru), with the addition of four Fluorine atoms, gives the best overall performances at the largest value of the bias considered (up to 2 Volts). On the other hand, the non-symmetric species RuOs and RuFe upon Fluorine substitution, are characterized by more stable but slightly smaller rectification. The main reason for this behaviour lies in the increase of the electronic charge stabilization introduced by the substituents and already observed in purely organic molecular rectifiers.[5]

4.4 Diarylethene-based molecular switch

Another electronic device which can be reproduced with molecules is the switch, where the electron flow, which can be mono- or bi-directional, can be activated (ON) or deactivated (OFF) through an external action (gate). Usually, molecular switches are three-terminal devices where the external stimulus can be electrical, given by a voltage applied to the gate,[97,98] or even optical, providing that the molecule is photo-active. In this case the energy of the incident

radiation can be used to change the conformation of the molecule, from one conducting to another non-conducting, and vice-versa. When the switching functionality is activated by an external optical radiation, we speak of molecular optical switches. These species undergo a reversible transformation between two stable states characterized by different absorption spectrum and the two isomers also show different equilibrium geometry and/or physical properties.

This is the case of species based on azobenzene[97,99–101] or diarylethene groups,[97,100,102–106] where the easiness of controlling their reversibility at the molecular level, and their fast response time versus the input optical signal can be a significant advantage in view of possible technological use in real devices. Indeed, there are already promising applications in molecular memories[107] and studies which point out the possibility of building transistor-like devices[108] using optically active molecules.

Here, we focus on diarylethenes, where a variation on the conductance can be expected as a consequence of the photo-induced rearrangement of single and double bonds inside the central ring (Fig. 4.17). This class of molecules has, in fact, two isomers: one with a C-C open bond and one with the same bond closed. By irradiation with UV light the open form give rises to the closed form, which in turn transforms back in the open form by visible light irradiation.

Experimentally[105,106] open and closed forms have been found to exhibit different conductivity, in relation to the different setup of π-bonds. We want then to investigate the switching mechanism in these class of systems by using the FOXY method described previously. In particular, we are interested in the TSC and 4Py species (see Fig. 4.17), as defined in the original work of Briechle *et al.*, which are shown to have an "ON" state with a current of two orders of magnitude higher than the "OFF" state.

The computed I/V curves for the TSC and 4Py species, both in open and closed state, are reported in Fig. 4.18. For both systems we find a much higher conduction for the closed form (Fig. 4.17). The current is found larger, both in the ON and in the OFF state,

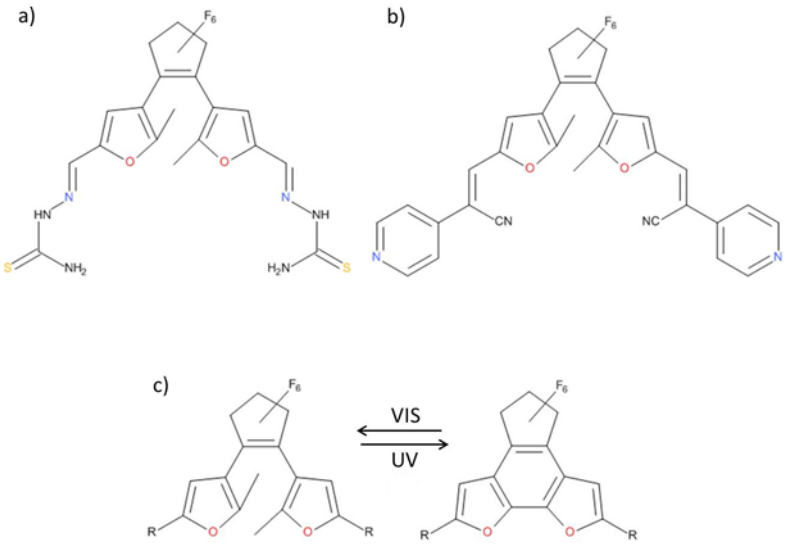

Figure 4.17: a) TSC and b) 4Py molecules. c) open and closed form of the diarylethene unit with oxygen instead of the usual sulphur.[106] The diarylethene unit changes, reversibly, between open and closed form via visible and UV radiation. R indicates a generic end-group.

for the 4Py species and at small bias we can recognize an Ohmic behavior which agrees with the experiments.[105] The I/V curves also show slightly asymmetric currents for positive and negative voltages, as the asymmetry of the molecules found in the geometrical optimization would suggest, especially in the open state.

As far as the 4Py species is concerned, this is in accordance with the experiments,[105] whereas for the TSC system, the literature data available seems to give different and contrasting results. In fact, while in Ref.[105] the TSC system is shown to behave as the 4Py, with the closed state conducting and the open one not, in Ref[106] the reported data are the opposite, with the open state conducting and the closed one not.

The I/V behavior of Fig. 4.18 can be explained by looking at the transmission spectra of Fig. 4.19, where, as outlined before, the Fermi level is taken in the middle of the HOMO-LUMO orbital energies (red vertical line in the figures). The orbitals which have significant projection onto the terminal Gold electrodes fragments (Q_L and Q_R terms in Eq. 3.66) and thus give rise to peaks in the transmission function inside the bias window are the HOMO, LUMO and LUMO+1. The conduction is then of electron-hole type.

For the TSC species, LUMO and LUMO+1 provide the largest contribution in the T(E) spectra, with a wide band generated by the broadening of these two levels, whereas for the 4Py species the contribution of the three orbitals appears more balanced. The HOMO plays a slightly most important role in the conduction mechanism, especially for positive bias: the 4Py transmission function shows three peaks, with the ones assigned to HOMO and LUMO+1 at the same intensity.

The difference in the $T(E)$ between the open and the closed forms of both TSC and 4Py species is rather evident: the peaks are at least one order of magnitude smaller in the open case. This, according to Eq. 3.26, results in the small or negligible current observed for the open forms. In particular, for the open TSC system, the shift of the bands of T(E) is such that only a small part of them fall in the integration range (dashed vertical lines) and the current is then

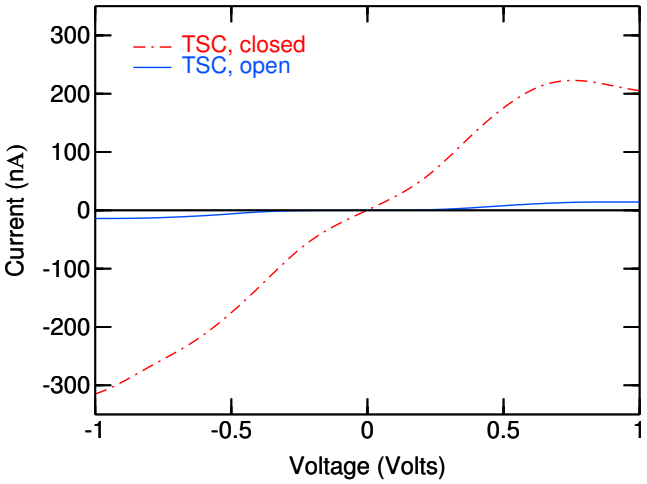

(a) TSC

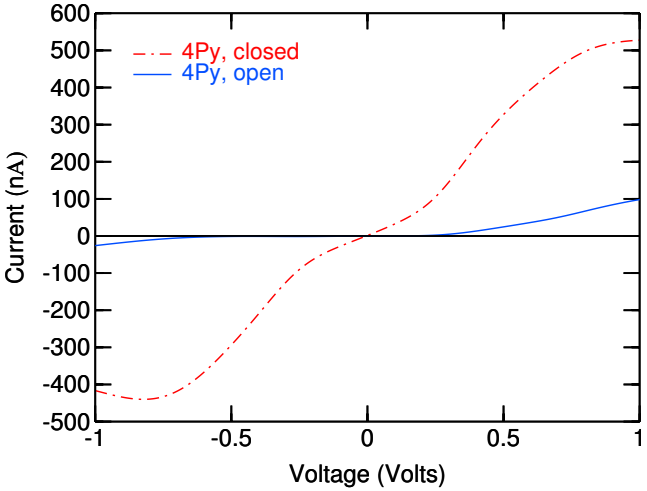

(b) 4Py

Figure 4.18: Current/Voltage characteristics of the TSC (left) and 4Py (right), both in the ON and OFF state.

even much lower in value. On the other hand, we should also notice that the applied field has a negligible effect on the MOs of the closed species: their energy position is almost the same at either -1V, 0V and +1V (especially in the 4Py case). This means that there is no significant polarization effect at the origin of the observed I/V characteristics and the small rectification effect observed find an explanation in the little changes of the peak intensities.

Further insights on the transport properties of the two species can be obtained by a closer look at the shape of the molecular orbitals which are relevant for the conduction mechanism. In Fig 4.20, HOMO, LUMO and LUMO+1 at 0V for the TSC and 4Py molecules, either in the open and closed states, are reported. We can see that in the ON state (closed form) the MOs, are essentially delocalized in the whole molecule, with significant component on both the terminal Au fragments: the HOMO has the largest molecule-type character, whereas the virtual ones have mostly Gold character. When the external radiation, opening the central bond of the diarylethene moiety, switches the system from the closed to the open (OFF) state, the MOs near the Fermi level loose their delocalized character and become localized separately in the left and right parts of the extended molecule. As a consequence of this lack of a communication channel, electrons cannot flow between left and right electrodes and the transmission function becomes very small.

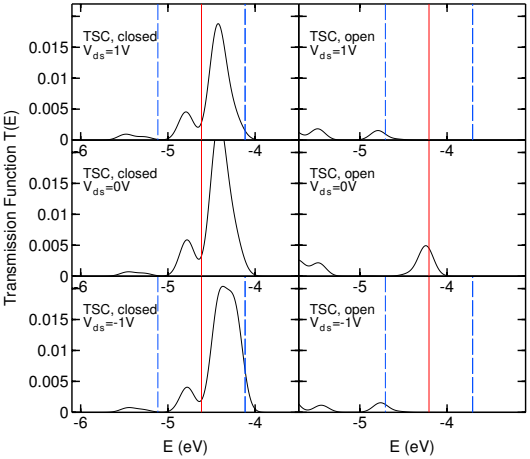

(a) TSC

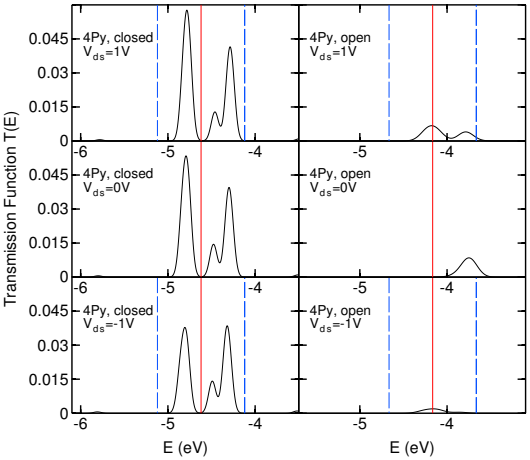

(b) 4Py

Figure 4.19: Transmission function of the TSC (top) and 4Py (bottom) species, both in "open" (right column) and "closed" (left column) conformation, at +1V, 0V and −1V. Vertical red line: Fermi level of the species. Vertical blue lines: integration range, as in Eq. 3.26

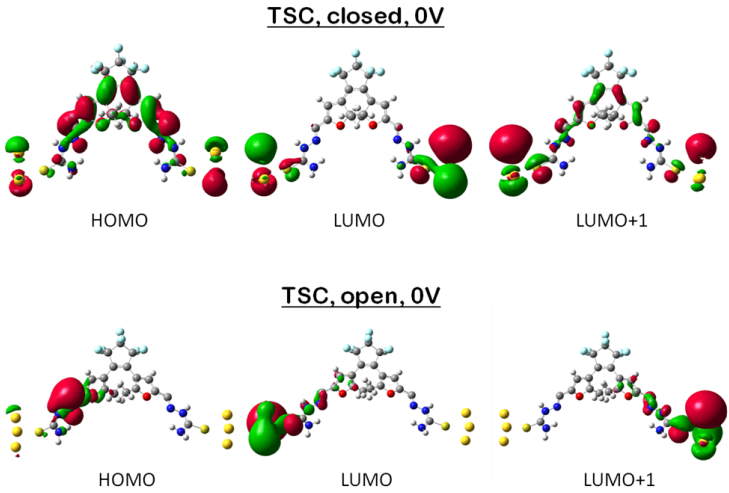

(a) TSC

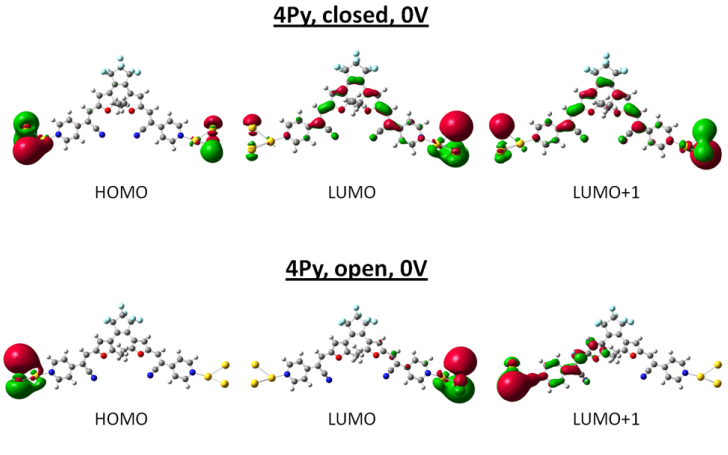

(b) 4Py

Figure 4.20: MOs of the TSC (top) and 4Py (bottom) molecule relevant for the conduction in the range, at 0V (Au=yellow, C=grey, H=white,N=bark blue, O=red, S=olive, F=light blue).

Chapter 5

Conclusions

In this Thesis, the work done in the three years of PhD activity at Scuola Normale Superiore and ICCOM/CNR in Pisa has been summarized. The subject of the Thesis was the study of electronic transport properties of various types of molecules which can mimic fundamental circuit elements, in particular rectifiers and switches, by a computational approach based on the Non-Equilibrium Green's Function (NEGF) method and the Landauer-Büttiker theory, in order to understand the physical mechanism under the rectifying/switching behaviour of the molecules under study.

We have been able to clearly define a computational route capable of a rapid evaluation of transport properties of various molecules sandwiched between electrodes, by means of an approximated Landauer-NEGF-DFT method. The main idea is that transport properties are dependent on the projection of the molecular orbitals onto a suitable terminal fragment of the molecule under study: the metallic leads are not considered explicitly (which is mandatory in standard NEGF-DFT-Landauer codes), except for the terminal fragments made by a 3-atom Gold cluster, which realize an appropriate chemical environment for the molecular bridge. The main draw-

back here is some loss in the precision of the computed data, mostly from the assumptions made in order to make the method rapid and computationally feasible, but also due to the unavoidable problems connected with DFT (mainly regarding self interaction and positioning of virtual orbitals, including the fact that DFT is a ground-state theory). All the transport calculations are done without the need of a complete self consistent transport calculation (such as the one described in Chapter 3). All the equations obtained from the model described in Section 3.3 have been implemented in our domestic FOXY code, which is also, up to now, completely interfaced with the GAUSSIAN suite of programs.

With this method at hand, the first step was to calibrate the whole method, finding a value for the Δ parameter (the only "empirical" parameter that enters the model), by reproducing the benzene 1,4 dithiol experimental I/V characteristics. We found that the best value for the parameter was $\Delta = 0.0015$. After the calibration, we reproduced the transport properties of the molecular rectifier described by Weber *et al.*[5] We were able to reproduce the experimental I/V curves, defining the value of the central torsional angle of the probed molecule, and to understand the rectification mechanism: the rectification mainly comes from asymmetries due to the presence of the fluorine atoms, which generate an excess of charge in the rightmost benzene ring that is easily driven into the right electrode when a negative bias is applied to the two-terminal structure.[78]

We also analysed the properties of binuclear compounds of transition metals (to our knowledge, never synthesised), in order to understand if only a variation of one of the two metal atoms used in these complexes could asymmetrise the I/V characteristics of these species, or if the presence of substituents is also required. Current/voltage characteristics, obtained with a combination of GAUSSIAN's DFT calculation together with transport properties with the FOXY code, show that, in the $\pm$2V regime, for unsubstituted species, the rectification effect is very low, and usually very dependent on the operating voltage (with the best value of 1.2 for the Ru-Os species). This is

a direct consequence of the fact that current onset voltages for positive and negative biases are different, depending on the transition metals in the species: whereas for negative voltages the onset of the current is always almost the same (due to the fact that, in the left part of the species there is always a Ru metal atom), for positive voltages the onset of the current varies depending on the transition metal present in the center of the porphyrazine moiety. We also find that the rectification effect, mainly driven by occupied frontier orbitals, is opposite to the Aviram-Ratner model. The introduction of substituents, in the form of four Fluorine atoms on the rightmost pyrazine ring, essentially stabilizes the rectifying behaviour over a broader range of voltages, slightly increasing the rectification ratio for every species (with Ru-Ru-F species as the best case, with a value of 3 for almost all the entire voltage range). We also find that the effect of the Fluorine atoms is the same that we previously found for the Weber diode, that is charge stabilization on a localized region of the entire molecule, which is easily dragged to the electrode by an external longitudinal electric field.[88]

We have then investigated charge transport in the TSC and 4Py photochromic species, based on a central sulfur-free diarylethene core, as synthesized in Refs.[105,106] The behavior observed experimentally for these photochromic switches can be reproduced within the framework of the FOXY code. All the main features of the experimental I/V curves, and especially the switching effect, can be found in the results of our computations. This has allowed us, for the TSC and 4Py molecules in both open and closed state, to give an explanation at the molecular level of the observed characteristics, through an investigation of the transmission functions and of the shape of the orbitals relevant in the charge transport. The peaks in the transmission functions are assigned to HOMO, LUMO and LUMO+1 orbitals, which are delocalized in the closed state and strongly localized, either on the left or right part of the molecule, in the open state. Localized orbitals cannot provide good transmission channels for the electron to tunnel from one electrode to the other, mainly because, as in our model, these orbitals, do not have signifi-

cant components on both left and right Au fragments and therefore do not provide $Q_L Q_R$ products sufficiently large to contribute to the transmission function (Eq. 3.66).

5.1 Future perspectives

Even if the FOXY code has proven to be useful and quite effective in understanding and predicting transport properties of molecular species of interest, a lot of work is still needed in order to improve the effectiveness of the overall code. Several issues should be addressed:

- Although the FOXY code uses a simplified treatment for calculating transmission functions and I/V characteristics, it still needs a separate calculation for every voltage steps used in order to build the full I/V characteristics. If the scope of the code is to offer a tool for rapid calculations of transport properties (to make the fast "screening" of different molecule possible), at the price of a slight reduction in the overall precision of the calculations, further approximations in order to treat the external field are still necessary. One idea (described in[57]) is to calculate the response to an external field in an effective way. Given Approx. 1 of Chapter 2 as granted, the field generates an electronic polarization across the transport direction (in our case, the long axis of the molecule), which in some way reflects on the values of the projections of the MOs onto the terminal fragments. Therefore, it can affect the transmission properties.
  The one-electron effective Hamiltonian of the molecule in the presence of an uniform electric field can be written as:

$$\widehat{H}_M = \widehat{T} + \widehat{V}_N + \widehat{F} \cdot \boldsymbol{r} + \widehat{G}[\rho] \tag{5.1}$$

  where $\widehat{T}$ is the kinetic energy operator, $\widehat{V}_N$ is the nuclear attraction potential operator and $\widehat{G}$ is an operator that includes

electron repulsion, the exchange and correlation terms. We define

$$\Delta\rho = \rho - \rho_0 \tag{5.2}$$

the variation on the electronic density due to the perturbation $\widehat{F}\cdot\boldsymbol{r}$. Other than the usual three approximation we introduced for the FOXY method (see Section 3.3), we can then employ a new additional approximation:

Approximation 4 *We can neglect $\Delta\rho$ in the nonlinear term $\widehat{G}$ and use the value $\widehat{G}[\rho_0]$ for every value of the field $\widehat{F}$. This can be viewed as an expansion of the $\widehat{G}$ operator in a power series of $\Delta\rho$, retaining only the zero-th order term.*

$\widehat{H}_M$ then becomes linear and does not require a self-consistent procedure.The field dependent MOs φ_j can be computed with a simple diagonalization in the basis of the unperturbed MOs.[109] Since this approximation leads to a small "excess" in response, because the $\Delta\rho$ effect is against the effect induced by the potential connected to the electric field, a "reducing factor" for the field is needed in order to overcome such problem.
We define $\Delta\mu$ as the molecular dipole moment induced by the field (via a self-consistent calculation). $\Delta\mu_a$ is the same quantity, but obtained using $\widehat{G}[\rho_0]$. From that, we can compute polarizabilities:

$$\Delta\mu = \alpha F \tag{5.3}$$

$$\Delta\mu_a = \alpha_a F \tag{5.4}$$

We can rewrite the first relation as

$$\Delta\mu = \alpha_a \left(\frac{\alpha}{\alpha_a}\right) F \tag{5.5}$$

In this way, it is possible to obtain the correct change in the dipole moment by using the approximate polarizability α_a and

a "reduced" field. Then, one can use

$$\widehat{H}_M = \widehat{T} + \widehat{V}_N + \left(\frac{\alpha}{\alpha_a}\right) \widehat{F} \cdot \overrightarrow{r} + \widehat{G}[\rho] \tag{5.6}$$

where α and α_a are obtained with a single calculation with the field included, to obtain the molecular orbitals to be used in the evaluation of the self-energies, the projections onto the terminal fragment and the transmission function. Such procedure needs to be tested for the newer version of the FOXY code. In particular, it is crucial to define up to what voltage (or better, fields) such an approximation can hold. It is not necessary to reach high voltages during calculations (such as, for example, $\pm$5V), mainly for two reasons: first, high electric field tends to completely destroy the metal/molecule/metal junction and the molecule itself (especially for long molecules), second, there is a trend in integrated circuit design which tends to reduce the reference voltage used in microcircuits, for power consumption reasons.

- Regarding the problem of the position of the Fermi level of the metallic contact, the inclusion of more atoms into the fragments could provide a more accurate description of the molecule-lead interaction. Straightforward addition of Au atoms to the fragments has proven to be infeasible: first for the fact that DFT calculation on such structures are cumbersome and hard to converge, second, because the way in which the FOXY code treats electric fields leads to wrong results if bigger leads are used. In fact, GAUSSIAN DFT applies an electric field acting on every atom of the extended molecule, which is incorrect, since we want a field acting only in the proper molecular region. The atoms in the leads represents only the electrodes, seen in our method as plates of a capacitor, and not part of the molecule to be probed. The problem of bigger leads is strongly entwined with the field as treated in the FOXY code. Apply-

ing a constant electric field to the molecule (with also the lead fragments included) means that we are, in fact, applying a bias also to the metal chunk which represents the electrode, leading to fake results in the I/V curve. A more rigorous way would be the solving of the Poisson equation for the junction, with metal Fermi levels (shifted by an external bias) as boundary conditions. Of course, this would require the definition of a 3D energy grid for the solution of the Poisson equation, and an efficient Poisson solver, all of them linked with the main FOXY routine. Another possibility could be to work directly in the GAUSSIAN code, introducing a new way in which an external potential can be added directly to certain selected atoms. The idea here is to insert in the total Hamiltonian of the system a potential term acting only on the lead atoms, according to $\mu_L = \varepsilon_f - V/2$, $\mu_R = \varepsilon_f + V/2$, $eV = (\mu_L - \mu_R)$. After this passage, a regular DFT calculation can start, obtaining, after convergence of the calculation, a more precise response of the molecule to the external bias.

- Even if Landauer-Büttiker theory has proven to be successful in assessing transport properties of molecules and, more in general, nanostructures, it has its foundations on some approximations that could lead to wrong results.[52,53] This is due to the fact that we "close" the problem in an effective way (via self-energies), and that we treat an intrinsically dynamical problem with static scattering theory (we move the electrons across the junction, one by one, without considering many-body interactions at all). More than that, the molecule-contact interfaces are not yet well understood.

These are the main issues in order to better generalize the whole theory behind the FOXY code.

Appendices

Appendix A

Green's Function

We define a single-particle Hamiltonian, which contains a kinetic part $\widehat{H}_0$ and a time-independent potential part $\widehat{V}$ which encapsulates all the scattering due to the junction itself. we can then write it as:

$$\widehat{H}_S = -\frac{\hbar^2}{2m}\nabla^2 + V(\mathbf{r}) \tag{A.1}$$

with $\widehat{H}_0 = -\frac{\hbar^2}{2m}\nabla^2$ and $\widehat{V} = V(\mathbf{r})$. We can then solve two types of Schrödinger equations: one for the full Hamiltonian $\widehat{H}_S$

$$i\hbar\frac{d|\Psi(t)\rangle}{dt} = \widehat{H}_S|\Psi(t)\rangle = (\widehat{H}_0 + \widehat{V})|\Psi(t)\rangle \tag{A.2}$$

and a similar one for the kinetic part of the total Hamiltonian

$$i\hbar\frac{d|\Psi(t_0)\rangle}{dt} = \widehat{H}_0|\Psi(t_0)\rangle \tag{A.3}$$

We can recognize that the equations A.2 and A.3 are of the type

$$\widehat{L}\psi(t) = f(t) \tag{A.4}$$

with $\widehat{L}$ of the form:

$$\widehat{L} = i\hbar\frac{d}{dt} - \widehat{H} \tag{A.5}$$

with $\widehat{H}$ either $\widehat{H}_S$ or $\widehat{H}_0$. We can now define the *Green's function* or *propagator* $\widehat{G}(t)$ for the linear, time-independent, Hermitian, differential operator $\widehat{L}$ as the solution of the equation:

$$\widehat{L}\widehat{G}(t) = \widehat{I}\delta(t) \tag{A.6}$$

To this equation there are two corresponding solutions, which define two different types of Green's functions:

$$\left(i\hbar\frac{\partial}{\partial t} - \widehat{H}_S\right)\widehat{G}^{\pm}(t) = \widehat{I}\delta(t) \tag{A.7}$$

with boundary conditions:

$$\begin{array}{ll} \widehat{G}^{+}(t) = 0, & t < 0 \\ \widehat{G}^{-}(t) = 0, & t > 0 \end{array} \tag{A.8}$$

We call $\widehat{G}^{+}$ *retarded Green's function* and $\widehat{G}^{-}$ *advanced Green's function*. Now, we can observe an important relation: if we take, for example, the solution for the retarded Green's function

$$\widehat{G}^{+}(t) = \begin{cases} -\dfrac{i}{\hbar}\exp\{-i\dfrac{\widehat{H}_S t}{\hbar}\} & t > 0 \\ 0 & t < 0 \end{cases} \tag{A.9}$$

we can see that it is proportional to the common time-evolution operator $\widehat{U}(t, t_0)$ for time-independent Hamiltonians. It is possible, then, to rewrite the usual equation for the evolution of the state vector $|\Psi(t)\rangle$ using the Green's function:

$$|\Psi(t)\rangle = i\hbar\widehat{G}^{+}(t - t_0)|\Psi(t_0)\rangle \tag{A.10}$$

which is valid for times $t > t_0$. It is clear now that the retarded Green's function propagates in time the state vector, for times later

than the starting one. It is possible to get the advanced Green's function in a same fashion:

$$\widehat{G}^{+}(t) = \begin{cases} 0 & t > 0 \\ \dfrac{i}{\hbar}\exp\{-i\dfrac{\widehat{H}_S t}{\hbar}\} & t < 0 \end{cases} \tag{A.11}$$

and describe the state vector with:

$$|\Psi(t)\rangle = i\hbar\widehat{G}^{-}(t-t_0)|\Psi(t_0)\rangle \tag{A.12}$$

valid for times $t < t_0$. In this formulation, we can describe the state vector in past times t with respect to the "present" time t_0. It is also important to highlight an important relation:

$$\left[\widehat{G}^{+}(t)\right]^{\dagger} = \widehat{G}^{-}(-t) \tag{A.13}$$

The time-independent versions of all these relation can be obtained by Fourier transform of the time-dependent Green's functions (it is necessary to introduce some infinitesimal ϵ in order to guarantee convergence for the integrals):

$$\widehat{G}^{+}(E) = \mathcal{F}\left[\widehat{G}^{+}(t)\right] \int_0^{+\infty} e^{iEt/\hbar} e^{-\epsilon t/\hbar} \widehat{G}^{+}(t)dt \tag{A.14}$$

$$\widehat{G}^{-}(E) = \mathcal{F}\left[\widehat{G}^{-}(t)\right] \int_0^{+\infty} e^{iEt/\hbar} e^{+\epsilon t/\hbar} \widehat{G}^{-}(t)dt \tag{A.15}$$

These equation can be recast using A.9 and A.11. Usually, at this stage, a new complex number is introduced: $z = E + i\epsilon$ for the retarded Green's function and $z = E - i\epsilon$ for the advanced Green's function, so both the equations can be rewritten as;

$$\widehat{G}(z) = \frac{\widehat{I}}{z - \widehat{H}_S} \tag{A.16}$$

It is possible to redo all the passages for the kinetic part of the total Hamiltonian alone ($\widehat{H}_0$): first, extracting the time-dependent

Green's functions for this term (in its retarded and advanced form), then, doing a Fourier transform of the results. In the end, it is possible to get (using again $z = E + i\epsilon$ for the retarded solution and $z = E - i\epsilon$ for the advanced one):

$$\widehat{G}_0(z) = \frac{\widehat{I}}{z - \widehat{H}_0} \tag{A.17}$$

It is possible now to underline some properties of the time-independent formulation of the Green's functions. $\widehat{G}(z)$ is an analytical function in the complex plane, except in points or portions (branch cuts) of the real axis, in correspondence to the eigenvalues of $\widehat{H}_S$. For discrete eigenvalues, $\widehat{G}(z)$ has simple poles in correspondence to the bound spectrum eigenvalues. The inverse also holds: the poles of $\widehat{G}(z)$ give the bound spectrum of $\widehat{H}_S$. The branch cuts give the continuous spectrum of $\widehat{H}_S$ instead. Even in the time-independent formulation, A.13 holds.

Given the eigenstates of the Hamiltonian $\widehat{H}_S$, the Green's function can be expressed as:

$$\widehat{G}(z) = \sum_{E_i,\alpha} \frac{|\Psi_{E_i,\alpha}\rangle\langle\Psi_{E_i,\alpha}|}{z - E_i} + \sum_{\alpha} \int_0^{+\infty} \frac{|\Psi_{E,\alpha}\rangle\langle\Psi_{E,\alpha}|}{z - E} \tag{A.18}$$

which is called *spectral representation* of the Green's function.

Appendix B

Lippman-Schwinger Equation

In order to find the eigenfunctions of the operator $\widehat{H}_S = \widehat{H}_0 + \widehat{V}$, it is necessary to find the eigenfunctions of the "unperturbed" Hamiltonian $\widehat{H}_0$, express the Green's function $\widehat{G}$ (associated to the total Hamiltonian $\widehat{H}_S$) in terms of $\widehat{G}_0$ and $\widehat{V}$, and extract information about eigenvalues and eigenfunctions from the Green's function. It is usually easy to find $\widehat{G}_0$, given good information about $\widehat{H}_0$, and from $\widehat{G}$ information about eigenvalues and eigenfunctions are readable from the poles and the corresponding residues.

Equations A.16 and A.17 gives us an expression for the Green's functions associated to $\widehat{H}_S$ and $\widehat{H}_0$ respectively. Since $\widehat{H}_S = \widehat{H}_0 + \widehat{V}$,

we can write:

$$\begin{aligned}\widehat{G}(z) &= (z-\widehat{H}_0-\widehat{V})^{-1} \\ &= \left\{\left(z-\widehat{H}_0\right)\left[\widehat{I}-\left(z-\widehat{H}_0\right)^{-1}\widehat{V}\right]\right\}^{-1} \\ &= \left[\widehat{I}-\left(z-\widehat{H}_0\right)^{-1}\widehat{V}\right]^{-1}\left(z-\widehat{H}_0\right)^{-1} \\ &= \left[\widehat{I}-\widehat{G}_0(z)\widehat{V}\right]^{-1}\widehat{G}_0(z)\end{aligned} \tag{B.1}$$

We can now expand in power series:

$$\begin{aligned}\frac{\widehat{I}}{\widehat{I}-\widehat{G}_0\widehat{V}} &= \sum_{n=0}^{+\infty}\left(\widehat{G}_0\widehat{V}\right)^n \\ &= 1+\widehat{G}_0\widehat{V}+\widehat{G}_0\widehat{V}\widehat{G}_0\widehat{V}+\ldots\end{aligned} \tag{B.2}$$

and rewrite:

$$\begin{aligned}\widehat{G}(z) &= \widehat{G}_0+\widehat{G}_0\widehat{V}\widehat{G}_0+\widehat{G}_0\widehat{V}\widehat{G}_0\widehat{V}\widehat{G}_0+\ldots \\ &= \widehat{G}_0+\widehat{G}_0\widehat{V}\widehat{G} \\ &= \widehat{G}_0+\widehat{G}\widehat{V}\widehat{G}_0\end{aligned} \tag{B.3}$$

Equation B.3 is called *Lippman-Schwinger equation*, which relates $\widehat{G}$ to $\widehat{G}_0$ and to $\widehat{V}$. The eigenstates are then easily obtained:

$$\left(E-\widehat{H}_0\right)|\Psi\rangle = \widehat{V}|\Psi\rangle \tag{B.4}$$

$$\begin{aligned}|\Psi^{\pm}(E)\rangle &= |\Psi_0^{\pm}(E)\rangle+\widehat{G}_0^{\pm}(E)\widehat{V}|\Psi^{\pm}(E)\rangle \\ &= |\Psi_0^{\pm}(E)\rangle+\widehat{G}^{\pm}(E)\widehat{V}|\Psi_0^{\pm}(E)\rangle\end{aligned} \tag{B.5}$$

which are also called *Lippman-Schwinger equation*. In this equation, $|\Psi_0^{\pm}(E)\rangle$ represents solution associated to the retarded and advanced Green's function (as a result of the scattering process introduced by the scattering potential $\widehat{V}$), which are originated from a initial state $|\Psi_0^{\pm}(E)\rangle$ (non-interacting multi-particle state in the distant past, eigensolution of the Hamiltonian $\widehat{H}_0$).

Acknowledgment

Poco piú di tre anni fa, dopo la laurea specialistica, decisi di intraprendere l'esperienza del dottorato, in un campo non propriamente "affine" a quello che era il mio curriculum ingegneristico. A Pisa trovai fortunatamente la possibilitá di proseguire lungo la strada che ero deciso a percorrere.

Innanzitutto, un ringraziamento va al Prof. **Vincenzo Barone**, che ha permesso che questa bella esperienza fosse possibile, fornendomi mezzi adeguati, interessanti spunti nei momenti in cui il lavoro sembrava arenato, e permettendomi di lavorare nell'ambito che piú mi interessava in un ambiente stimolante e altamente competente.

Il mio lavoro non si é strettamente svolto nelle strutture della Scuola Normale, ma al CNR, precisamente all'istituto ICCOM, a stretto contatto con il Dott. **Alessandro Ferretti** e il Prof. **Ivo Cacelli**, che ringrazio entrambi per avermi sempre seguito, anche in momenti difficili, e per avermi fornito consigli, opinioni e in generale avermi insegnato perfettamente che cosa vuol dire fare il "mestiere del ricercatore", in tutte le sue sfaccettature (non solo accademiche).

Probabilmente non sarei arrivato alla fine di questo percorso se a fianco a me non avessi avuto la fortuna di trovare persone che, con un pizzico di orgoglio, sento di poter chiamarle AMICI (tutto rigorosamente in maiuscolo). A cominciare dai "colleghi" di Perfezionamento per finire a tutte quelle altre belle persone che ho conosciuto per le strade di Pisa nelle mie varie "scorribande" alla scoperta di

questa affascinante cittá.

Ringrazio quindi le primissime persone che ho conosciuto il giorno dell'esame di ammissione al Perfezionamento: **Daniele** e **Luciano**. Di strada ne abbiamo fatta parecchia, e in questi anni abbiamo condiviso gioie e dolori, dal primo istante, ma mi sembra che ce la siamo cavata bene... E poi, **Matteo**. In tre anni ne sono successe di cose, e sei stato un'ottima spalla sia ci fosse stato da piangere, che da ridere, o discutere di musica, di arte, di ragazze, di vita. Spero di aver ricambiato tutto quello che mi hai dato. Mi raccomando: "Piacere, Matteo" sempre e comunque.

Appena entrato alla Scuola, ho trovato altri due ragazzi alle prese col loro Perfezionamento: Filippo e Ivan. **Filippo**, mi ricorderó sempre le incredibili discussioni che sono nate dalle nostre differenze intrinseche, ma credo che particolarmente impresse mi rimarranno le squisite cene e soprattutto i post-cena a base di grappa: un vero toccasana! **Ivan**, anche a te un enorme "grazie", perch le varie parole, le sere in Vettovaglie o dove capitava, spese a districare il caos dei nostri pensieri non saranno dimenticate. Come non saranno mai dimenticati i tuoi ritardi e le tue multe per divieto di sosta: il comune di Pisa probabilmente ti far un monumento.

Vorrei quindi ringraziare **Nicola**, che ho conosciuto nel mio secondo anno di Perfezionamento. Siamo menti affine, "nerd" al punto giusto e non poteva che nascere una bella amicizia. Oltretutto, senza le sue fisime sulla tipografia, probabilmente questa tesi avrebbe un aspetto orrendo, come anche le slides della discussione...

Un ringraziamento anche a tutti gli altri Perfezionandi, **Franco**, i due **Danilo** e **Teresa** che, seppur vi conosca da poco, posso con sicurezza dire che siete delle grandi persone (Danilone, anche in senso letterale...).

Nello stesso piano degli uffici del Dreams, c'é anche il gruppo di Cosmologia. E anche qui devo ringraziare i miei amici **Serena** e **Andrea**. In particolare, Andrea va ringraziato anche per essere un DM "severo ma giusto". E poi, volevo anche ringraziare la terza dottoranda di Cosmologia, **Livia**: a volte la vita ti mette di fronte grandi persone e Livia é una di queste, e credo che, poi, persone cosí

non le perderai mai. Il peccato di Livia quello di essere un po' una "fava", ma le si pu perdonare pure questo.

Un grandissimo Grazie anche a tutti gli "stranieri" del gruppo: **Julien**, **Mireia**, **Corentin**, **Bala** perché avete colorato alcune delle serate migliori che ho passato a Pisa con la vostra simpatia irrefrenabile (... e qualche dozzina di birra comparsa casualmente sui tavoli. Sí, sto parlando a te, Corentin!).

Ma non é finita qui! A Pisa non ho conosciuto solo persone strettamente legate al mio dottorato. Ho incrociato e condiviso momenti bellissimi con parecchia gente, che mi preme di ringraziare perché anche loro sono state colonne portanti di questi tre anni.

Parto cronologicamente dalle prime persone che ho conosciuto, in una strana notte di festa alla Normale finita in disastro: **Pedro** e **Laura**. Siete persone grandissime, scienziati/artisti alla vostra bellissima maniera, e sono veramente fortunato ad avervi conosciuto. Ho condiviso con voi bevute, gite, viaggi, notti, avventure, suonate, riflessioni, giochi, pensieri, praticamente tutto! Vi voglio bene, ragazzi. E **Maurizio** e **Alice**, e tutta la mitica casa di Via La Maddalena, e tutte le cene, le giocate, i film, le risate, e in generale tutte le belle cose che lí sono successe, o da lí sono partite.

E poi **Andrea** (uomo del futuro), **Tommaso** (un grande!), **Roberto** (mitico Bob), **Daniele**, **Marta** (la miglior infermiera spagnola di Pisa) e, ultima ma non ultima, **Caterina** (figurati se non poteva comparire nei ringraziamenti di uno dei suoi "angeli custodi" di tesi!) Siete stati, tutti, senza eccezione, importantissimi per me. Un sorriso non posso che dedicarvelo.

E, ovviamente, un ringraziamento anche a mia **mamma** e mio **babbo**. Sono stati sempre presenti, con parole e gesti bellissimi, sia quando questo dottorato sembrava diventare difficile da sopportare, sia quando filava liscio. Mi hanno sempre incoraggiato in maniera incondizionata (e a volte ci si é anche scontrati un po'...), non chiedendo mai nulla in cambio e aiutandomi in tutte le maniere possibili. Saró sempre grato a loro per questo e per tutto quello che hanno fatto per me sinora. Vi voglio bene.

Concludo con un altro ringraziamento: a **Pisa**, alle sue giornate

e soprattutto alle sue notti, teatro perfetto per tre anni di vita appassionati e intensi.

Ancora, a tutti quanti quelli qui citati (e a quelli che mi sono dimenticato di ricordare, colpa mia!), dal cuore, **GRAZIE**.

Bibliography

[1] Moore, G. *Electronics* **1965**, *38*, 8.

[2] Feynman, R. *Eng. Sci.* **1963**, *23*, 22.

[3] Aviram, A.; Ratner, M. *Chem. Phys. Lett.* **1974**, *29*, 277.

[4] Chen, J.; Reed, M.; Rawlett, A.; Tour, J. *Science* **1999**, *286*, 1550.

[5] Elbing, M.; Ochs, R.; Koentopp, M.; Fischer, M.; von Hnisch, C.; Weigend, F.; Evers, F.; Weber, H.; Mayor, M. *PNAS* **2005**, *102*, 8815.

[6] Birge, R. *Molecular and Biomolecular Electronics*, Vol. ; Am. Chem. Soc., Washington DC, 1991.

[7] Di Ventra, M. *Electronic Transport Through Nanoscale Systems*, Vol. ; Cambridge University Press, 2008.

[8] Datta, S. *Quantum Transport: Atom to Transistor*, Vol. ; Combridge University Press, 2005.

[9] Cuniberti, G.; Fagas, G.; Richter, K. *Introducing Molecular Electronics*, Vol. ; Springer, 2005.

[10] Cuevas, J.; Sheer, E. *Molecular Electronics: An Introduction to Theory and Experiment*, Vol. ; World Scientific, 2010.

[11] Yao, Z.; Postman, H.; Balents, L.; Dekker, C. *Nature* **1999**, *402*, 273.

[12] Tans, S.; Verschueren, A.; C., D. *Nature* **1998**, *393*, 49.

[13] Collier, C.; Wong, E.; Belohradsky, M.; Raymo, F.; Stoddart, J.; Kuekes, P.; Williams, R.; Heath, J. *Science* **1999**, *285*, 391.

[14] Huang, Y.; Duan, X.; Cui, Y.; Lauhon, L.; Kim, K.-H.; Lieber, C. *Science* **2001**, *294*, 1313.

[15] Nitzan, A.; Ratner, M. *Science* **2003**, *300*, 1384.

[16] Lindsay, S.; Ratner, M. *Adv. Mater.* **2007**, *19*, 23.

[17] Kohn, W.; Sham, L. *Phys. Rev.* **1965**, *140*, A1133.

[18] Parr, R.; Yang, W. *Density Functional Theory of Atoms and Molecules;* Oxford University Press, 1989.

[19] Lang, N. *Phys. Rev. B* **1995**, *52*, 5335.

[20] Lang, N.; Avouris, P. *Phys. Rev. B* **2000**, *84*, 358.

[21] Landauer, R. *IBM J. Res. Dev.* **1957**, *1*, 233.

[22] Keldysh, L. *Zh. Eksp. Teor. Fiz.* **1964**, *47*, 1515.

[23] Kadanoff, L.; Baym, G. *Quantum Statistical Mechanics*, Vol. ; Benjamin,New York, 1962.

[24] Delaney, P.; Greer, J. *Phys. Rev. Lett.* **2004**, *93*, 036805.

[25] Strange, M.; Rostgaard, C.; Hkkinen, H.; Thygesen, K. *Phys. Rev. B* **2011**, *83*, 115108.

[26] Strange, M.; Thygesen, K. *Beilstein, J. NaOPTnotechnol.* **2011**, *2*, 746.

[27] Evers, F.; Weigend, F.; Koentopp, M. *Phys. Rev. B* **2004**, *69*, 235411.

[28] Krstic, P.; Dean, D.; Zhang, X.; Keffer, D.; Leng, Y.; Cummings, P.; Wells, J. *Comput. Mater. Sci.* **2003**, *28*, 321.

[29] Runge, E.; Gross, E. *Phys. Rev. Lett.* **1984**, *52*, 997.

[30] Petersilka, M.; Grossman, U.; Gross, E. *Phys. Rev. Lett.* **1996**, *76*, 1212.

[31] Renaud, N.; Ratner, M.; Joachim, C. *J. Phys. Chem. B* **2011**, *115*, 5582.

[32] Varga, K. *Phys. Rev. B* **2011**, *83*, 195130.

[33] Stefanucci, G.; Almbladh, C.-O.; Kurth, S.; Gross, E.; Rubio, S.; van Leeuwven, R.; Dahlen, N.; von Barth, U. *Lect. Notes in Phys.* **2006**, *706*, 479.

[34] Snchez, C.; Stamenova, M.; Sanvito, S.; Bowler, D.; Horsfield, A.; Todorov, T. *J. Chem. Phys.* **2006**, *124*, 214708.

[35] Tomfohr, J.; SanOPTkey, O. *Phys. Statu Solidi B* **2001**, *226*, 115.

[36] Di Ventra, M.; Todorov, J. *J. Phys. Cond. Matt.* **2004**, *16*, 8025.

[37] Zheng, X.; Wang, F.; Yam, C.; Chen, G. *Phys. Rev. B* **2007**, *75*, 195127.

[38] Ke, S.-H.; Liu, R.; Wang, W.; Baranger, H. *J. Phys. Cond. Matt.* **2004**, (16), 8025.

[39] Maciejko, J.; Wang, J.; Guo, H. *Phys. Rev. B* **2006**, (74), 085324.

[40] Cheng, C.-L.; Evans, J.; Voorhis, T. *Phys. Rev. B* **2006**, (74), 155112.

[41] Bushong, N.; Sai, N.; Di Ventra, M. *Nano Lett.* **2005**, (5), 2569.

[42] Sai, N.; N., B.; Hatcher, R.; Di Ventra, M. *Phys. Rev. B* **2007**, (75), 115410.

[43] Stefanucci, G.; Almbladh, C.-O. *Phys. Rev. B* **2004**, *69*, 195318.

[44] Baer, R.; Seideman, T.; Ilani, S.; Neuhauser, D. *J. Chem. Phys.* **2004**, (120), 3387.

[45] Henderson, T.; Fagas, G.; Hyde, E.; Greer, J. *J. Chem. Phys.* **2006**, (125), 244104.

[46] van Wees, B.; van Houten, H.; Beenakker, C.; Williamson, J.; Foxon, C. *Phys. Rev. Lett.* **1988**, *60*(9), 848–850.

[47] Xue, Y.; Datta, S.; Ratner, M. *Chem. Phys.* **2002**, *281*, 151.

[48] Damle, P.; Ghosh, A.; Datta, S. *Chem. Phys.* **2002**, *281*, 171.

[49] Stokbro, K.; Taylor, J.; Brandbyge, M.; Mozos, J.-L.; Ordejon, P. *Computational Material Science* **2003**, *27*, 151.

[50] Zahind, F.; Paulsson, M.; Datta, S.; Associated Press, 2003; Vol. .

[51] Yang, Z.; Lang, N.; Di Ventra, M. *Phys. Rev. B* **2003**, *82*, 233407.

[52] Evers, F.; Weigend, F.; Koentopp, M. *Phys. Rev. B* **2004**, *69*, 235411.

[53] Krstic, P.; Dean, D.; Zhang, X.; Keffer, D.; Leng, Y.; Cummings, P.; Wells, J. *Comput. Mater. Sci.* **2003**, *28*, 321.

[54] Toher, C.; Sanvito, S. *Phys. Rev. B* **2008**, *77*, 155402.

[55] Pemmaraju, C.; Archer, T.; Sanchez-Portal, D.; Sanvito, S. *Phys. Rev. B* **2007**, *75*, 045101.

[56] Toher, C.; Sanvito, S. *Phys. Rev. Lett.* **2007**, *99*, 056801.

[57] Cacelli, I.; Ferretti, A.; Girlanda, M.; Macucci, M. *Chem. Phys.* **2007**, *333*, 26.

[58] Gonzales, C.; Simon-Manso, Y.; Batteas, J.; Marquez, M.; Ratner, M.; Mujica, V. *J. Phys. Chem. B* **2004**, *108*, 18414.

[59] Wang, C.-K.; Fu, Y.; Luo, Y. *Phys. Chem. Chem. Phys.* **2001**, *3*, 5017.

[60] Anderson, P. *Phys. Rev.* **1961**, *124*, 41.

[61] Newns, D. *Phys. Rev.* **1969**, *178*, 1123.

[62] Mulliken, R. *J. Chem. Phys.* **1955**, *23*, 1833.

[63] Bergfield, J.; Solomon, G.; Stafford, C.; Ratner, M. *Nano Lett.* **2011**, *11*, 2759–2764.

[64] Yeganeh, S.; Ratner, M.; Galperin, M.; Nitzan, A. *Nano Lett.* **2009**, *5*, 1770–1774.

[65] Herrmann, C.; Solomon, G.; Ratner, M. *J. Am. Chem. Soc.* **2010**, *132*, 36823684.

[66] Zahid, F.; Ghosh, A.; Paulsson, M.; Polizzi, E.; Datta, S. *Phys. Rev. B* **2004**, *70*, 245317.

[67] Frisch, J.; Trucks, G.; Schlegel, H.; Scuseria, G.; Robb, M.; Cheeseman, J.; Scalmani, G.; Barone, V.; Mennucci, B.; Petersson, G.; Nakatsuji, H.; Caricato, M.; Li, X.; Hratchian, H.; Izmaylov, A.; Bloino, J.; Zheng, G.; Sonnenberg, J.; Hada, M.; Ehara, M.; Toyota, K.; Fukuda, R.; Hasegawa, J.; Ishida, M.; Nakajima, T.; Honda, Y.; Kitao, O.; Nakai, H.; Vreven, T.; Montgomery, J.; Peralta, J.; Ogliaro, F.; Bearpark, M.; Heyd, J.; Brothers, E.; Kudin, K.; Staroverov, V.; Kobayashi, R.; Normand, J.; Raghavachari, K.; Rendell, A.; Burant, J.; Iyengar, S.; Tomasi, J.; Cossi, M.; Rega, M.; Millam, J.; Klene, M.; Knox, J.; Cross, J.; Bakken, V.; Adamo, C.; Jaramillo, J.;

Gomperts, R.; Stratmann, R.; Yazyev, O.; Austin, A.; Cammi, R.; Pomelli, C.; Ochterski, J.; Martin, R.; Morokuma, K.; Zakrzewski, V.; Voth, G.; Salvador, P.; Dannenberg, J.; Dapprich, S.; Daniels, A.; Farkas, O.; Foresman, J.; Ortiz, J.; Cioslowski, J.; Fox, A. *Gaussian Development Version, Gaussian, Inc., Wallingford CT,* **2009**.

[68] Mujica, M.; Ratner, M.; Nitzan, A. *Chem. Phys.* **2002**, *28*, 147.

[69] Zazza, C.; Amadei, A.; Sanna, N.; Aschi, M. *Chem. Comm.* **2008**, page 3399.

[70] Andrews, D.; Solomon, G.; Van Duyne, R.; Ratner, M. *J. Am. Chem. Soc.* **2008**, *130*, 17319.

[71] Tsuji, Y.; Staykov, A.; Yoshizawa, K. *J. Phys. Chem. C* **2011**, *116*, 2575.

[72] Meyer, J.; Wadewitz, A.; Lokamani.; Toher, C.; Gresser, R.; Leo, K.; Riede, M.; Moresco, F.; Cunberti, G. *Phys. Chem. Chem. Phys.* **2011**, *13*, 14421.

[73] Armstrong, N.; Rainer, C.; McDonagh, A.; Cortie, M.; Ford, M. *Nano Lett* **2007**, *7*, 3018.

[74] Asai, Y.; Nakamura, H.; Hihath, J.; Bruot, C.; Tao, N. *Phys. Rev. B* **2011**, *84*, 115436.

[75] He, H.; Pandey, R.; Mallik, G.; Karna, S. *J. Phys. Chem. C* **2009**, *113*, 1575.

[76] Franzen, S. *Chem. Phys. Lett.* **2003**, *381*, 315.

[77] Reed, M.; Zhou, C.; Muller, C.; Burgin, T.; J.M., T. *Science* **1997**, *278*, 252.

[78] Barone, V.; Cacelli, I.; Ferretti, A.; Visciarelli, M. *Chem. Phys. Lett.* **2012**, *549*, 1–6.

[79] Creutz, C.; Taube, H. *J. Am. Chem. Soc.* **1969**, *91*, 3988.

[80] Stokbro, K.; Taylor, J.; Brandbyge, M.; Mozos, J.-L.; Ordejon, P. *Computational Material Science* **2003**, *27*, 151.

[81] Brandbyge, M.; Mozos, J.-L.; Ordejn, P.; Taylor, J.; Stokbro, K. *Phys. Rev. B* **2002**, *65*, 165401.

[82] Hay, P.; Wadt, W. *J. Chem. Phys.* **1985**, *82*, 299.

[83] D'Alessandro, D.; Keene, F. *Chem. Rev.* **2006**, *106*, 2270.

[84] Stuzhin, P.; Vagin, S.; Hanack, M. *Inorg. Chem.* **1998**, *37*, 2655.

[85] Kim, S.-J.; Matsumoto, M.; Shigehara, K. *Synthetic Metals* **1999**, *107*, 27–33.

[86] Craciun, M.; Rogge, S.; der Boer, M.-J.; Margadonna, S.; Prassides, K.; Iwasa, Y.; Morpurgo, A. *Adv. Mater.* **2006**, *18*, 320.

[87] Givaja, G.; Amo-Ochoa, P.; Gomez-Garcia, C.; Zamora, F. *Chemical Society Reviews* **2012**, *41*, 115–147.

[88] Barone, V.; Cacelli, I.; Ferretti, A.; Visciarelli, M. *Phys. Chem. Chem. Phys.* **2013**, *15*, 11409–11419.

[89] Matsuura, Y. *J. Chem. Phys.* **2013**, *138*, 014311.

[90] Pan, J.; Zhang, Z.; Deng, X.; Qiu, M.; Guo, C. *Appl. Phys. Lett.* **2011**, *98*, 013503.

[91] Tsuji, Y.; Staykov, A.; Yoshizawa, K. *J. Phys. Chem. C* **2012**, *116*, 2575.

[92] Pipek, J. an Mezey, P. *J. Chem. Phys.* **1989**, *90*, 4916.

[93] Metzger, R. *Chem. Phys.* **2006**, *326*, 176–187.

[94] Scott, G.; Chichalk, K.; Peters, A.; Stoddart, J.; Hjiang, H. *Phys. Rev. B* **2006**, *74*, 113404.

[95] Reichert, J.; Ochs, R.; Beckmann, D.; Weber, H.; Mayor, M.; Löhneysen, H. *Phys. Rev. Lett* **2002**, *88*, 176804.

[96] Stokbro, K.; Taylor, J.; Brandbyge, M. *J. Am. Chem. Soc.* **2003**, *125*, 3674–3675.

[97] van der Molen, S. J.; Liljeroth, P. *J. Phys. Condens. Matter* **2010**, *22*, 133001.

[98] Song, H.; Reed, M. A.; Lee, T. *Adv. Mater.* **2011**, *23*(14), 15831608.

[99] Beharry, A. A.; Woolley, G. A. *Chem. Soc. Rev.* **2011**, *40*, 44224437.

[100] Kudernac, T.; Katsonis, N.; Brwne, W. R.; Feringa, B. L. *J. Mater. Chem.* **2009**, *19*, 71687177.

[101] Henzi, J.; Puschnig, P.; Ambrosch-Draxl, C.; Schaate, A.; Ufer, B.; Behrens, P.; Morgenstern, K. *Phys. Rev. B* **2012**, *85*(3), 035410.

[102] Cheng, H.-B.; Zhang, H.-Y.; Liu, Y. *J. Am. Chem. Soc.* **2013**, *135*(28), 1019010193.

[103] Uchida, K.; Yamanoi, Y.; Yonezawa, T.; Nishihara, H. *J. Am. Chem. Soc.* **2011**, *133*(24), 92399241.

[104] Simo, C.; Mas-Torrent, M.; Casado-Montenegro, J.; Otn, F.; Veciana, J.; Rovira, C. *J. Am. Chem. Soc.* **2011**, *133*(34), 1325613259.

[105] Kim, Y.; Hellmuth, T. J.; Sysoiev, D. adn Pauly, F.; Pietsch, T.; Wolf, J.; Erbe, A.; Huhn, T.; Groth, U.; Steiner, U. E.; Scheer, E. *Nano Lett.* **2012**, *12*(7), 37363742.

[106] Briechle, B. M.; Kim, Y.; Ehrenreich, P.; Erbe, A.; Sysoiev, D.; Huhn, T.; Groth, U.; Scheer, E. *Beilstein, J. NaOPTnotechnol.* **2012**, *3*, 798–808.

[107] Uchida, K.; Saito, M.; Murakami, A.; Kobayashi, T.; Nakamura, S.; Irie, M. *Chem. Eur. J.* **2005**, *11*, 534–542.

[108] Gilat, S. L.; Kawai, S. H.; Lehn, J. M. *Chem. Eur. J.* **1995**, *1*, 275–284.

[109] Langhoff, P.; Karplus, M.; Hurst, R. *J. Chem. Phys.* **1966**, *44*, 505.

List of Figures